People's Democratic Republic of Algeria
Ministry of Higher Education and Scientific Research
University M'Hamed BOUGARA – Boumerdès

Institute of Electrical and Electronic Engineering
Department of Electronics

Final Year Project Report Presented in Partial Fulfilment of
the Requirements for the Degree of

MASTER

In **Telecommunication**

Option: **Telecommunications**

Title:

Design of Compact Dual-Band Fractal Antennas for WLAN/WiMAX Applications

Presented by:

- **Hanane DROUICHE**

Supervisor:

- **Dr. Kahina DJAFRI**

Registration Number……/2024

Dedication

I dedicate this work to my lovely parents, their prayers, unconditional love and unwavering faith in me were and still a shield that protect and support me through the valleys and hills of my life. Words can barely express my gratitude for them. To my brother louai and sisters for their endless support and love which have been a bedrock of my strength and a source of unending inspiration. to all my big family and friends. I am deeply honored to dedicate this humble work for you all.

Acknowledgments

First and foremost, I'm thankful to Allah, the most gracious, the most merciful for helping me to complete this work. It is my belief in Him that guided me through the hardest times when it seemed impossible to go on. Secondly, I would like to express my deepest gratitude to my supervisor "Dr. K Djafri" for her help, guidance, patience, motivation and support. Her guidance helped me in all the time of research and writing of this report.

Abstract

In this project, a new design approach is presented for achieving a miniaturized dual-band microstrip patch antenna (MPA) suitable to be used for 2.4 GHz WLAN band, and 5.5 GHz WiMAX band. The first proposed antenna which is composed of a semi-circular radiating arm attached to four identical smaller semicircular arms to form a comb structure loaded with a horizontal rectangular stub with a 50-Ω transmission by feed line printed on the top side of an FR4 substrate. A tapered partial ground plane is printed on the back side of the substrate. The second proposed design is composed of three interconnected ω −shaped arms feed with a 50 Ohm microstrip line on the top side of the FR-4 substrate and a tapered ground plane in its back side. A CST Microwave Studio (CST MWS) is used to model the designed antennas, and simulation results, in terms of reflection coefficient (S11), realized peak gain, efficiency and radiation patterns. To validate the design concept, the antenna designs are fabricated, the simulated and measured S11 results are nearly coincide with each other. The semi-circular comb antenna is characterized by miniaturized size of 24 × 29.5 mm^2, and measured bandwidths of 600 MHz (2–2.6 GHz) and 2.6 GHz (5.4–8 GHz). The second proposed structure, triple ω −shaped patch, is characterized by compact size of 22 × 32 mm^2, and measured bandwidths of 800 MHz (2–2.8GHz) and band 2.4 GHz (4-6.4 GHz).

Table of Content

List of Figures

List of Tables

List of Abbreviations

MPA	Microstrip Patch Antenna
CST	Computer Simulation Technology
2D	Two Dimensional
3D	Three Dimensional
WLAN	Wireless local area network
WiMAX	Worldwide Interoperability for Microwave Access
BW	Bandwidth.
FNBW	First Null Beamwidth.
HPBW	Half Power Beamwidth
FR-4	Flame Resistant 4.
GSM	Global System for Mobile communication.
MSA	Microstrip antenna.
RFID	Radio Frequency Identification.
SMA	SubMiniature Version A.
VNA	Vector Network Analyzer.
VSWR	Voltage Standing Wave Ratio.
IBM	International Business Machines Corporation.

List of Symbols

ϵ_r	Relative Permittivity.
h	Substrate Thickness.
Γ	Reflection Coefficient.
S11	Scattering Parameter (Reflection Coefficient).
Zin	The Input Impedance of the Antenna.
R_{in}	The Real Part (resistance) of the Input Impedance
X_{in}	The Imaginary Part (reactance).
Z_0	The Characteristic Impedance of the Transmission Line.
f_H	Low Cutoff Frequency.
f_L	High Cutoff Frequency.
D	Directivity.
Dmax	Maximum Directivity.
(θ, ϕ)	Radiation Intensity.
U0	Average Radiation Intensity.
Pin	Total Input (Accepted) Power.
Prad	Radiated Power.
$G(\theta, \phi)$	Gain
e_0	Radiation Efficiency.
Rr	Active or Radiation Power in The Far Field.
ϕ	The Elevation Angle.
θ	The Azimuth Angle.
dB	Decibel Scale.
dBi	Decibels Relative to Isotropic.

General Introduction

The rapid increase in mobile users, subscriber demands, and various enabling technologies of next-generation mobile and wireless communication systems have triggered antenna researchers to develop various antenna types, such as microstrip antennas, which stand out as fundamental devices [1].

This applications such as Wireless Local Area Network (WLAN) and Worldwide Interoperability for Microwave Access (WiMAX) are widely used. Each of these applications operates on different frequency bands so that the integration of dual-band antennas has become essential.

The fractal antenna is one of microstrip antenna types that has attracted notice. It utilize complex geometric shapes that repeat at different scales. This unique design approach endows fractal antennas with several advantageous properties, including multi-band functionality, reduced size, and improved radiation patterns. These characteristics make fractal antennas highly suitable for integration into dual-band systems, where they can significantly enhance antenna parameters [2].

In this work two dual-band fractal antennas are designed, simulated and fabricated so that this report includes three main chapters organized as follows:

- In Chapter 1, some of the basic notions of antennas in general besides special features of microstrip antennas, their privileges and applications, and an overview about the fractal antennas are presented.
- In Chapter 2, the design and analysis of comb-shaped dual-band fractal antenna operating at the bands [2.3 GHz-2.82 GHz] and [4.94 GHz -7.3 GHz] is investigated. This structure has evolved from semicircular-shaped microstrip line to a comb-shaped fractal antenna loaded with a rectangular stub. At each stage a parametric study is carried out to observe the effect of each geometrical parameter on reflection coefficient. Current distribution and radiation pattern are also simulated and studied. Finally, the fractal comb antenna is fabricated and measured and a comparison between the simulated and the measured results is presented.
- In Chapter 3, the design and analysis of a compact dual-band antenna with overall size of 32 x 22mm^2 is presented. The dual band operation is achieved by connecting three

identical ***ω***-shaped radiating strips while the compact size is resulted from the fractal geometry. The proposed structure comprises three interconnected ***ω***-shaped radiating branches. The dimensions of the branches are varied to cover the desired operating frequency bands, 2.4/5.2/5.8 GHz WLAN bands and 5.5 GHz WiMax band and to achieve compact size. The simulated impedance bandwidths of the proposed structure extend 2.24 GHz to 2.76 GHz for the first band whereas the second operating band ranges from 4.05 GHz to 6.89 GHz, which covers largely the intended applications. The simulated radiation pattern at both resonant frequencies is omnidirectional in the H-plane and dipole-like radiation in the E-plane. Finally, the proposed antenna is fabricated and tested to validate the used technical approach. A comparison between the simulated and measurement results is conducted and the results are in good agreement.

A conclusion is presented at the end of the report.

Chapter One
Generalities on Microstrip Antennas

Generalities on Microstrip Antennas

1.1 Introduction

Antennas are metallic structures that transmit and/or receive radio electromagnetic waves, converting radio frequency (RF) fields into alternating current or vice versa. With the advancement of wireless communication systems, Microstrip Patch Antennas (MPAs) are in great demand for both commercial and military applications. Multi-band and wideband antennas are desirable in personal communication systems, small satellite communication terminals, and other wireless applications. In this chapter, we will present the basics of microstrip patch antennas and an overview on fractal antennas.

1.2 Microstrip Antennas

Microstrip antennas are small antennas that consists of a conducting patch of any geometrical shape on one side of a dielectric substrate with relative dielectric constants typically ranging from 2.2 to 12, with a ground plane on the other side, as shown in Figure 1.1.

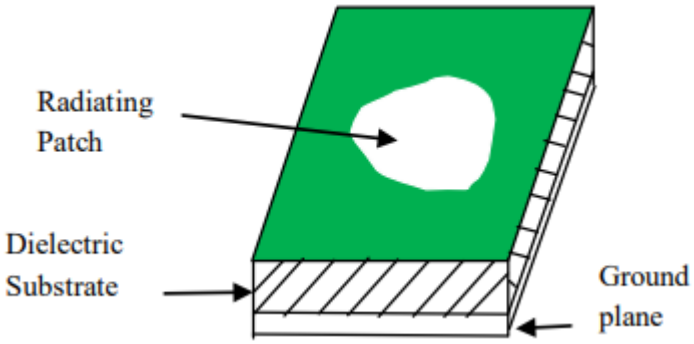

Figure 1.1 Basic structure of MPA [3]

1.3 Feeding Techniques

Microstrip antennas can be fed through various methods, which can be categorized into two main groups: contacting and non-contacting. In the contacting approach, RF power is directly supplied to the radiating patch through a connecting strip such as a microstrip line. Conversely, in the non-contacting method, power transfer between the microstrip line and the radiating patch is accomplished through electromagnetic field coupling. The choice of feeding technique is determined by the efficiency of power transfer among the radiation structure, feeding structure, and their impedance matching [4].

1.3.1 Microstrip Line Feed

In this technique, a conducting strip is connecting the patch to its feed line as shown in Figure 1.2 and the feed can be etched on the same substrate to provide a planar structure. However, as the thickness of the dielectric substrate being used, increases, surface waves and spurious feed radiation also increases, which hampers the bandwidth of the antenna. The feed radiation also leads to undesired cross polarized radiation [4]. This method of feeding is very widely used because it is very simple to design and analyze, and very easy to manufacture.

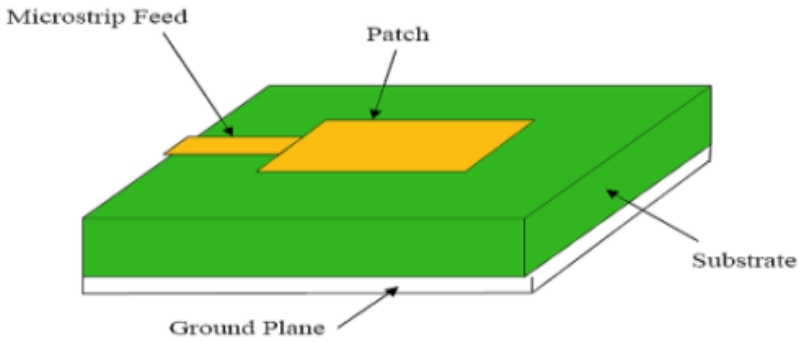

Figure 1.2 Microstrip line feed for rectangular patch [5].

1.3.2 Coaxial Feed

The coaxial feed, or probe feed, is a very common technique used for feeding microstrip patch antennas. In this method, the inner conductor of the coaxial cable is attached to the radiating patch, while the outer conductor is connected to the ground plane, as illustrated in Figure 1.3. This technique has low spurious radiation and is easy to fabricate and match. However, it has a narrow bandwidth and it is difficult to model especially for thick substrates.

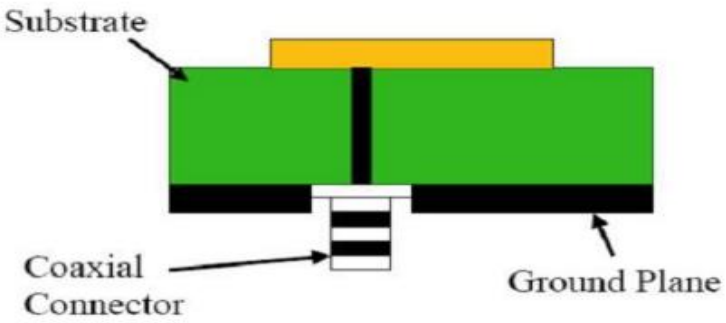

Figure 1.3 Coaxial feed [6].

1.3.3 Proximity Feed

This feeding technique is also known as electromagnetic coupling. Proximity coupling involves using two substrate. The patch is placed on the top, with the ground plane at the bottom, and a microstrip line connected to the power source lies between the two substrates, as shown in Figure 1.4. The main advantage of this feeding technique is that it eliminates spurious feed radiation and provides a very high bandwidth due to the overall increase in the thickness of the MPA [4].

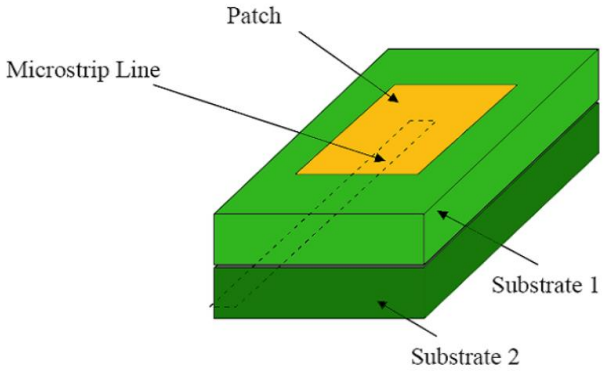

Figure 1.4 Proximity coupling [6].

1.3.4 Aperture Feed

In this technique, the radiating patch and the microstrip feed line are separated by the ground plane ,as shown in Figure 1.5. Coupling between the patch and the feed line is made through a slot or an aperture in the ground plane [7]. This type of coupling gives wider bandwidth[5].

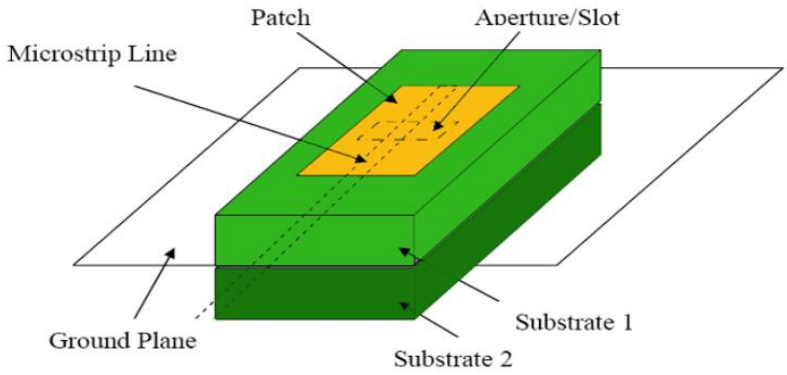

Figure 1.5 Aperture coupling [6].

1.4 Methods of Analysis

1.4.1 Transmission Line Model

Transmission Line Modelling states that the patch is considered as a transmission line with radiations along the length only with no consideration of the orthogonal direction of the propagation, and it result from the fringing fields at the patch extremities [8]. It is considered the simplest model but the least efficient one and the non-suitable for coupling feeds.

1.4.2 Cavity Model

Cavity model is more accurate and complex way compared to the previous one where the region between the patch and the ground plane is treated as a cavity, which is surrounded by the electric walls on the top and the bottom surface and the magnetic walls on the periphery. As the substrate used is thin as compared to wavelength inside the dielectric medium, the fields inside the cavity remain uniform along the thickness of the substrate while the equivalent magnetic current around the periphery computes the far fields and the radiation [8].

1.5 Basic Antenna Parameters

To more explain microstrip antenna performance, basic antenna parameters are listed in the following sections.

1.5.1 Input Impedance

The input impedance is the ratio of the voltage to current at the pair of the input antenna terminals, or the ratio of the appropriate components of the electric to magnetic fields at a certain point. It is represented as follows:

$$Z_{in} = R_{in} + jX_{in} \qquad 1\text{-}1)$$

Where R_{in} is the real part (resistance) of the input impedance, and X_{in} is the imaginary part (reactance).

1.5.2 Impedance Bandwidth

The impedance bandwidth is the frequency range for which the antenna is well matched to its feed. The impedance bandwidth can be measured by the characterization of the voltage standing wave ratio (VSWR) at the frequency band of interest. VSWR is a measure of impedance matching and how efficiently RF power is transmitted from a power source into a load through a transmission line, its practical value must not exceed 1.3 and the ideal case is

when $VSWR$ =1. The higher VSWR, the greater is the mismatch between the antenna and the feeding system, and is defined as:

$$VSWR = \frac{1 + |\Gamma|}{1 - |\Gamma|} \qquad 1\text{-}2)$$

Where Γ is the reflection coefficient at the terminals of the antenna and it is defined by:

$$\Gamma = \frac{Z_{in} - Z_0}{Z_{in} + Z_0} \qquad 1\text{-}3)$$

Where Z_0 is the characteristic impedance of the transmission (feed) line

The BW is usually determined from the graph of the reflection coefficient by the intersecting the -10 dB level or line with the S11 graph as illustrated in Figure 1.6 bellow.

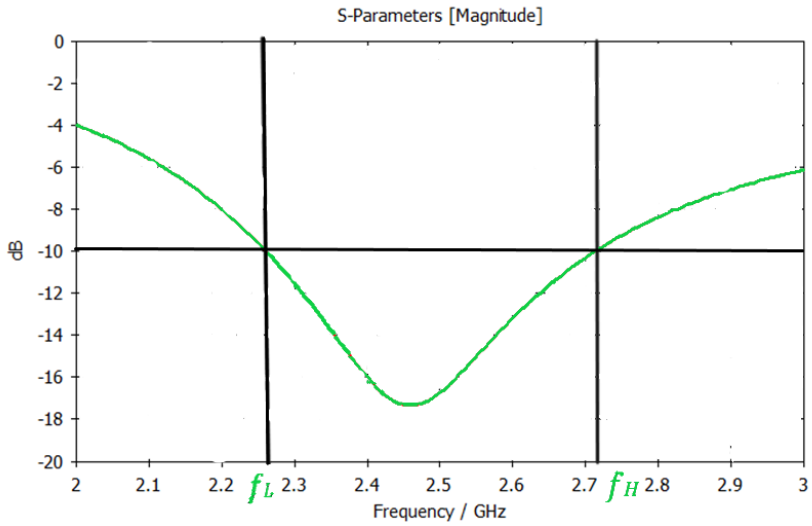

Figure 1.6 Bandwidth from a graph of reflection coefficient.

The expression used to calculate the bandwidth is:

$$BW = f_H - f_L \qquad 1\text{-}4)$$

Where f_H is the high cut-off frequency and f_L is the low one.

1.5.3 Directivity

The directivity of an antenna is a measure of how much the power emitted is concentrated in a given direction. The directivity of the antenna is always taken with respect to a known antenna, which is usually an isotropic radiator. On rare occasions, sometimes a half-

wavelength dipole is used as a reference. Mathematically, the directivity of an antenna is defined as:

$$\mathrm{D} = \frac{U(\theta,\phi)}{U_0(\theta,\phi)} = \frac{4\pi U(\theta,\phi)}{P_{rad}} \qquad 1\text{-}4)$$

Where:

$U(\theta,\phi)$: radiation intensity (W/unit solid angle).

$U_0(\theta,\phi)$: radiation intensity of an isotropic source (W/unit solid angle).

P_{rad}: total radiated power (W)

If the direction is not indicated, the maximum radiation direction is considered which implies the maximum directivity and equation 1.5 becomes:

$$\mathrm{D} = \frac{4\pi U_{max}}{P_{rad}} \qquad 1\text{-}6)$$

1.5.4 Gain

The gain is a parameter that is unique for each type of antenna and it is closely related to the directivity but it also takes into account the efficiency of the antenna that will be defined in the next section. the gain is the ratio of the radiation intensity in a certain direction to that resulted from an isotropic antenna radiation of the input power. Transforming this into equation would give [9]:

$$G(\theta,\phi) = \frac{4\pi U(\theta,\phi)}{P_{in}} \qquad 1\text{-}7)$$

Where:

$G(\theta,\phi)$ is the gain.

P_{in} is the total input power

1.5.5 Efficiency

The total antenna efficiency e_0 is used to take into account losses at the input terminals and within the structure of the antenna. Such losses may be due to reflections because of the mismatch between the transmission line and the antenna, and I^2R losses (conduction and dielectric) [9], with equation given below

$$e_0 = e_r e_c e_d \quad (1\text{-}8)$$

Where:

e_r: reflection (mismatch) efficiency.

e_c: conduction efficiency.

e_d: dielectric efficiency.

The conduction and dielectric losses of an antenna are very difficult to compute and in most cases they are measured. Even with measurements, they are difficult to separate and they are usually lumped together to form the e_{cd} efficiency as shown in

$$e_{cd} = e_c e_d \quad (1\text{-}9)$$

1.5.6 Radiation Pattern

A radiation pattern is a graphical representation of an antenna's radiation parameters as a function of spatial coordinates [9]. That is, the design of the antenna determines how the antenna radiates or receives energy into space. As it radiates in space, the radiation pattern is three-dimensional, and it is frequently expressed utilizing the principle plane patterns, which can be formed by cutting two slices across the 3D pattern at the pattern's highest value or by direct measurement. These basic plane designs are known as antenna patterns. The pattern are composed of lobes, a major lobe, side lobes, minor lobe and back lobe as shown in Figure 1.7.

1.5.7 Beamwidth

The beamwidth is defined as the angular separation between two identical points on opposite side of the pattern maximum as shown in Figure 1.7. Mainly two types of beamwidths exist which are:

Half Power Beam Width (HPBW) is defined by IEEE as: "in a plane containing the direction of the maximum of a beam, the angle between the two directions in which the radiation intensity is one-half the maximum value of the beam" [4].

First Null Beam Width (FNBW) is defined as the angular separation between the first null of the radiation pattern.

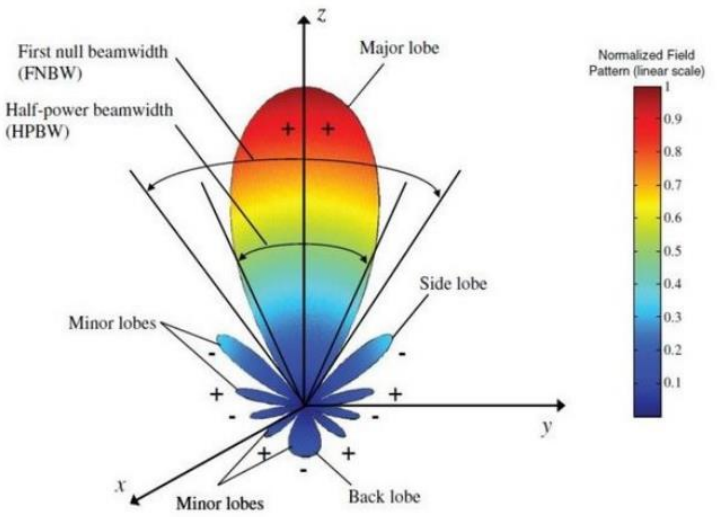

Figure 1.7 Antenna pattern's beamwidths and lobs [2].

1.5.8 Polarization

Polarization is the curve traced by the end point of the arrow (vector) representing the instantaneous electric field. The field must be observed along the direction of propagation [11]. There are three type of polarization , this types are illustrated in Figure 1.8.

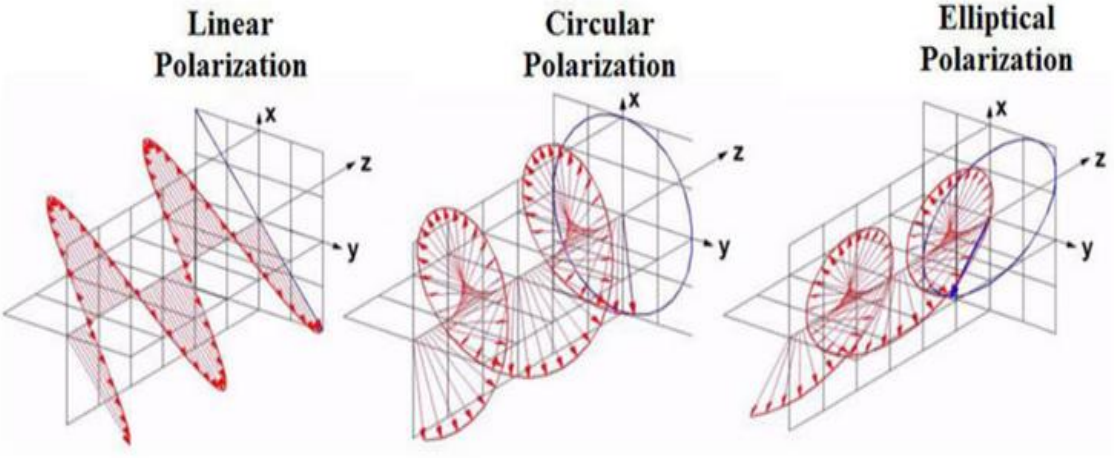

Figure 1.8 Linear, Circular and Elliptical polarizations

- **Linear polarization**

To say that an antenna is linearly polarized, the electric field (or magnetic field) vector must be constantly orients along the same straight line at every moment of time.

So the necessary and sufficient conditions to accomplish this is that the field must have two orthogonal linear components that must have the same magnitude, and same time-phase.

- **Circular polarization**

It is used to define a radio wave that rotates at a constant rate as the signal propagates while maintaining a constant magnitude. It has two types depending on the direction of rotation of the wave:

  - Right-Hand Circular Polarization (RHCP): when it is rotating to the right.
  - Left-Hand Circular Polarization (LHCP): when it is rotating to the left.

- **Elliptical polarization**

When the antenna is neither linearly nor circularly polarized, it is said to be of an elliptical polarization. It refers to an electric field that propagates in an elliptical helix. There can also be right-hand or left-hand elliptical polarization depending on the direction that the wave is propagating. In elliptical polarization, the two components of the field are not equal and they can differ in phase.

There are also terms co-polarization and cross-polarization are frequently used to describe the polarization purity of the linearly polarization antennas. Co-polar indicates the electric field component parallel to the polarization line, whereas, the cross-polar is the component perpendicular to it.

1.6 Antenna Advantages and Disadvantages

Microstrip antennas are often the preferred choice in many modern applications. However, their widespread use does not suggest they are devoid of drawbacks. The Table 1.1 will delineate both the advantages and disadvantages of these antennas.

Table 1.1 The advantages and disadvantages

Advantages	Disadvantages
Low profile	Low gain
Low weight	Low efficiency
Capable of dual and triple frequency operation	Narrow frequency bandwidth
Linear and circulation polarization	Excitation of surface waves
Feed lines and matching network can be fabricated simultaneously	Complex feed structures require high performance arrays

1.7 Microstrip Antennas Applications

The utilization of microstrip antennas is expanding across various fields and industries, particularly in commercial domains, owing to their cost-effectiveness in terms of substrate materials and fabrication. Some of their applications include:

- Worldwide Interoperability for Microwave Access (WiMax).
- Wireless local area network (LAN).
- Radar application.
- Satellite communication system.
- Direct broadcast television.
- Feed Elements in coaxial system.
- Global Positioning Systems (GPS).
- UHF patch antenna for space.
- Radio frequency identification (RFID).
- Telemedicine application.

1.8 Fractal Antennas

1.8.1 History

The word "fractal" comes from the Latin "fractus" which means "broken"[12]. In effect, a fractal is a geometric object "infinitely fragmented" whose details are observed to any chosen level. Although a number of fractal forms already known, the discovery of fractals is assigned to a French polytechnic, Benoit Mandelbrot (1924, 2010)[12]. His early research dating back to 1964 when he uses the term self-similar in a study conducted at international business machines corporation (IBM). But in 1975 he exhibited his work and gives the name "fractal" in his book "Les objects fractals" [12]. The original inspiration for the development of fractal geometry came largely from an in-depth study of the patterns of nature as seen in Figure 1.9 that represent an example which is plants in nature[12].

Figure 1.9 Fractals used to represnt plants in nature [9].

1.8.2 Definition

In general, a fractal is an object that starts with a simple geometry and makes a given number of scaled duplicates of the initial object at each iteration [13]. The geometry shown in Figure 1.10 is a fractal tree that is self-similar. The method used to create trees here begins with a trunk and allows one of its ends to branch off in two directions. Each of these branches is permitted to branch out again in the following iteration stage, and the process is repeated indefinitely.

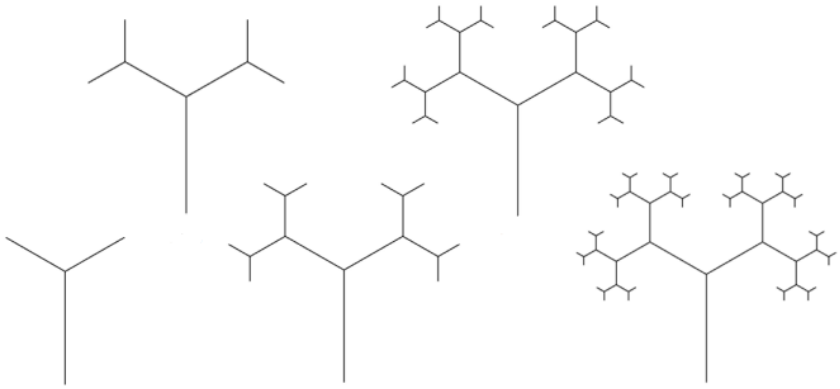

Figure 1.10 Various fractal binary tree iterations [13].

1.8.3 Properties

The fractal geometries are featuring two expected common properties, which are self-similarity and space filling properties. Both of these properties turn out to be a reason why fractals come out as an attractive way in designing antennas. Self-similarity properties interpreted as antenna which holds the duplication of itself at several scales and able to operate in similar way at several wavelength. This property allowing the wider band and reveal the multiband frequencies produced. The other one is space filling properties interpreted as reduction in antenna size which allow the antenna is fabricated smaller than elementary shape and attains the small surrounding space [11].

1.9 Conclusion

The principles of microstrip antennas were explained in this first chapter, along with a summary of fractal antennas. These concepts will be applied to the design of a comb-shaped dual-band fractal antenna with a stub loading in the second chapter.

Chapter Two
Design of a Comb-Shaped Dual Band Fractal Antenna

Design of a Comb-shaped Dual-Band Fractal Antenna

2.1 Introduction

This chapter presents a fractal dual-band antenna. The proposed structure is intended to operate in two bands, covering the 2.4 GHz WLAN and 5.5 GHz WiMAX bands.

CST Microwave Studio (CST MWS) is used to design the antenna and investigate the effect of its geometrical parameters.

2.2 Design Steps

In the process of reaching the final design and obtaining the desired results, the design of the patch went through different stages. The antenna structures are printed on an FR-4 substrate with a relative permittivity of ϵr = 4.3, a thickness of h = 1.6 mm, and a loss tangent of 0.025. The antennas are fed by a 50Ω −transmission line.

The following sections provide a step-by-step procedure, beginning with a semicircular antenna with specific dimensions, leading to the final structure of a fractal antenna loaded with a rectangular stub.

2.3 Semicircular-Shaped Microstrip Antenna

The proposed structure named 'Antenna 0' comprises of a semicircular radiating element with radius $S1$ attached to a 50Ω transmission line with width wf and length Lf printed in the front side of the FR-4 substrate. In the back side of the substrate a tapered ground plane with larger width of w, smaller width of wg1 and length wg as can be seen in Figure 2.1. The dimensions of the proposed design are summarized in Table 2.

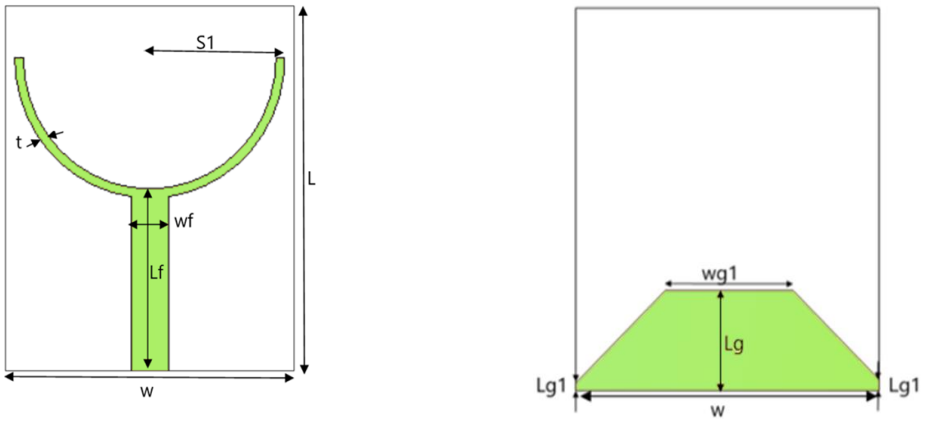

(a) (b)

Figure 2.1 the geometry of Antenna 0 (a)Front view (b)Bottom view

Table 2.1 The dimensions of the Antenna 0

Parameter	**S1**	**t**	**Lg**	**Lf**	**wf**	**Lg1**	**wg1**	**L**	**W**
Value (mm)	11	0.7	8	10.7	3	1	5	29.5	24

2.3.1 Simulated Reflection Coefficient

The simulated antenna reflection coefficient for the Antenna 0 is presented in Figure 2.2. It can be noticed that this proposed design operates in two frequency bands. The first operating band extends from 2.47 GHz to 3.09 GHz centered at 2.75 GHz with a reflection coefficient level of -21.95 dB while the second band extends from 7.92 GHz to 8 GHz with reflection coefficient level of -29 dB.

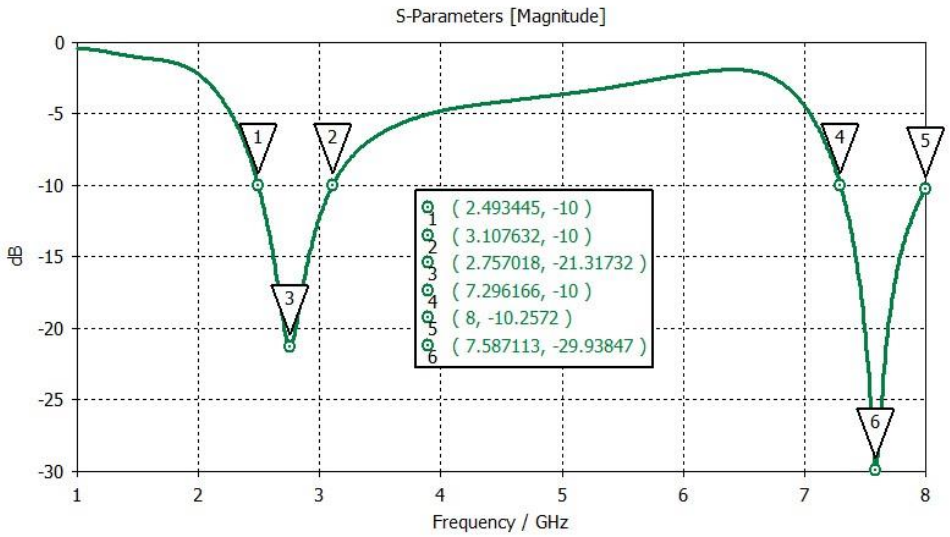

Figure 2.2 The reflection coefficient for Antenna 0

2.3.2 Parametric Study

To further investigate the proposed antenna performance, a parametric study is carried out and discussed.

- **Effect of varying the semicircular radius S1**

Figure 2.3 illustrates the simulated reflection coefficient results when the radius S1 is varied from 10 mm to 12 mm with a step of 1 mm. It is evident that as the value of S1 increases, the two frequency bands shift towards the lower frequency side. The considered value of S1 is 11 mm since it gives best impedance matching for both operating band

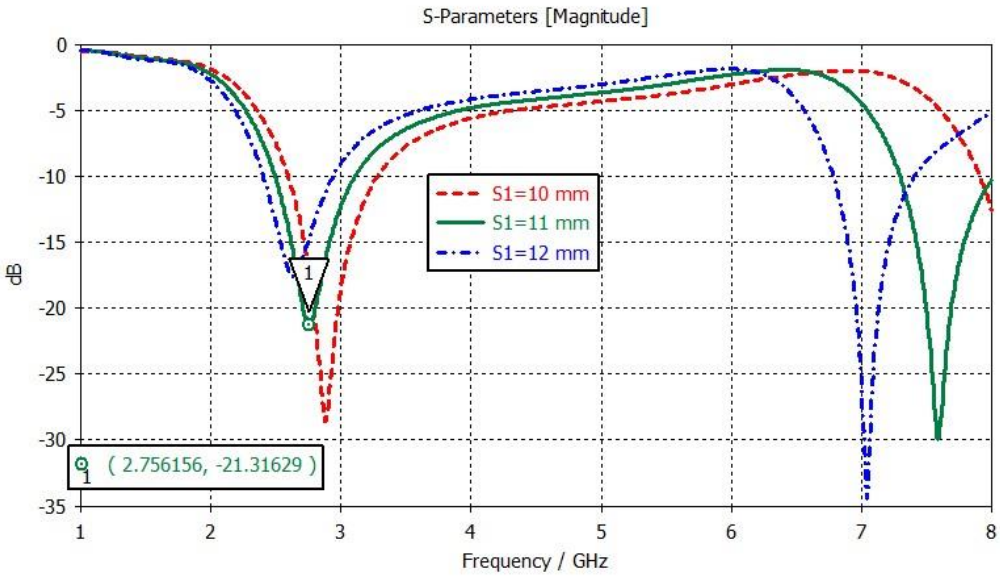

Figure 2.3 The effect of varying the radius S1 on the S1

2.4 First-Fractal Antenna Structure

To cover the 2.4 GHz WLAN and 5.5 GHz WiMAX bands, additional radiating elements need to be attached to the semicircular-shaped structure. As discussed in the fractal antenna section of the first chapter, the addition of scaled duplicates of the initial object can create additional bands. Therefore, two small semicircular-shaped arms with radius S2 are attached to the inner ends of the main semicircular branch and hence derive 'Antenna 1' as depicted in Figure 2.4. It is worth to mention that all the remained components and dimensions of the Antenna 1 are kept unchanged as compared Antenna 0.

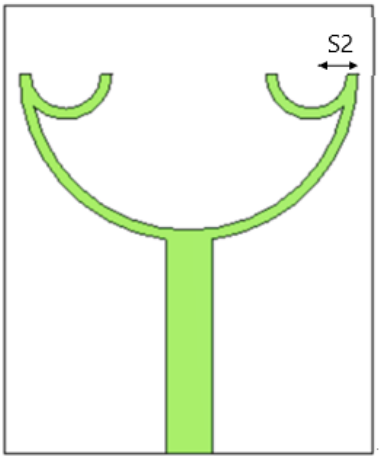

Figure 2.4 The geometry configuration of Antenna 1

2.4.1 Parametric Study

- **Effect of varying the semicircular radius S2**

Figure 2.5 illustrates the simulated reflection coefficient results when the radius S2 increases. It can be concluded from the results that the second operating frequency band decreases rapidly while the first frequency band is slightly shifted towards lower frequencies. The maximum value of S2 before overlapping of the antenna elements is 5.5 mm. It can be seen from the figure that the two intended bands are not achieved even for maximum value of S1. For this raison a second fractal stage need to be considered.

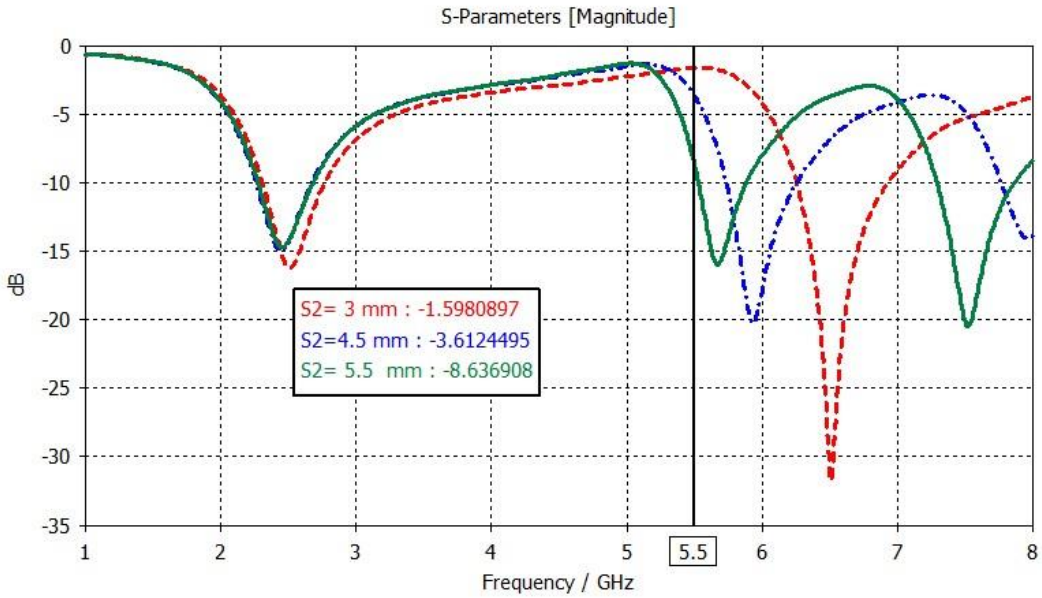

Figure 2.5 The effect of varying the radius S2 on the S11

2.5 Second-Stage Fractal Antenna Structure

With increasing the antenna dimensions, two additional semicircular branches, with radius S2 are attached to the inner ends of the radiating element of Antenna 1 to construct Antenna 2 as depicted in Figure 2.6.

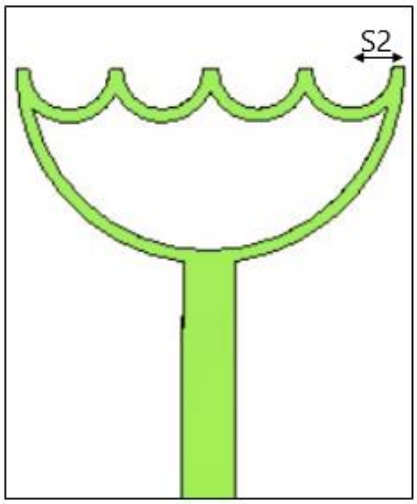

Figure 2.6 The geometry configuration of Antenna 2

2.5.1 Simulated Reflection Coefficient

Figure 2.7 shows the simulated reflection coefficient for Antenna 2. It can be observed that the second operating band extends from 5.3 GHz to 5.92 GHz, with a resonance at 5.51 GHz and a reflection coefficient level of -17.76 dB. The first band extends from 2.2 GHz to 2.6 GHz, with a resonance at 2.38 GHz and a reflection coefficient level of -15.84 dB.

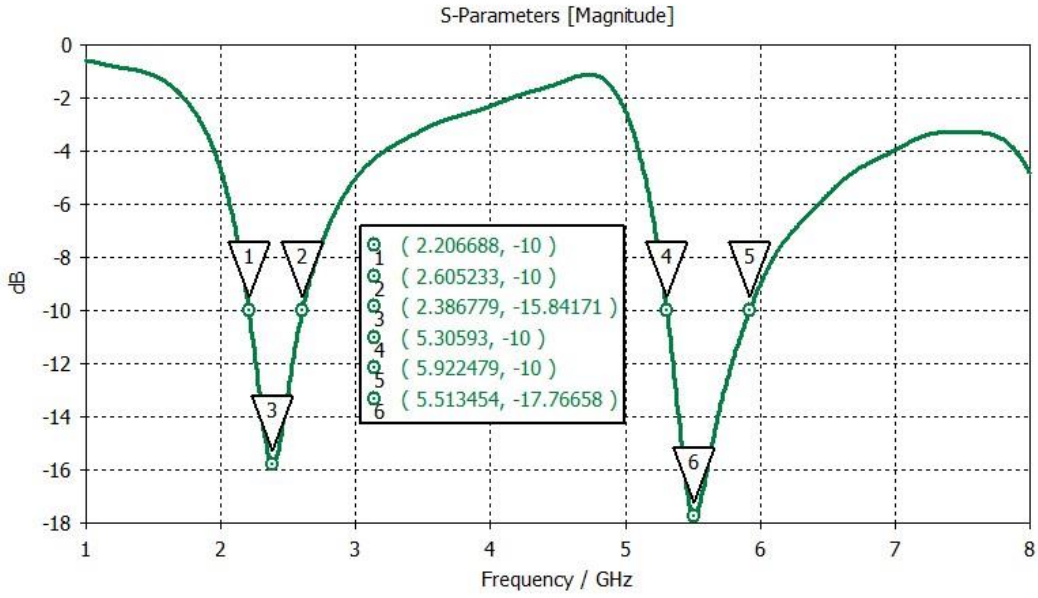

Figure 2.7 The reflection coefficient for Antenna 2

2.5.2 Parametric Study

- **Effect of radius of the semicircular-shaped branches S2**

The simulated results for S11 for different values of S2 are given in Figure 2.8. The results demonstrate that increasing S2 shifts the second band towards lower frequencies with decreased matching. The first band experiences a very small shift towards lower frequencies as well. It is observed that resonant frequency of the second band is centered at 5.5 GHz when S2 is 3 mm, which is the maximum value before overlap occurs between the small semicircles.

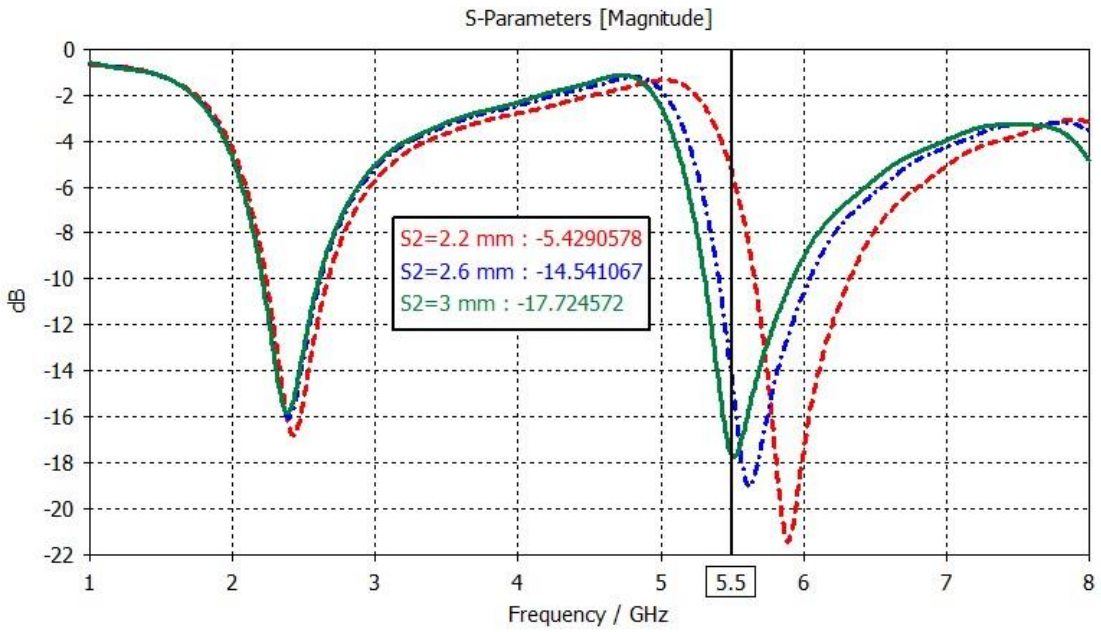

Figure 2.8 The effect of varying the radius S2 on the S11

- **Effect of varying the thickness th**

The simulated results for S11 for different values of th are presented in Figure 2.9.It can be seen that a thickness of 0.7 mm is the optimal choice since the best first and second resonant frequencies are centered at 2.45GHz and 5.5 GHz respectively. This thickness slightly affects the second band and almost no effect on the first band. Consequently, th allows a fine tune of the second resonant frequency.

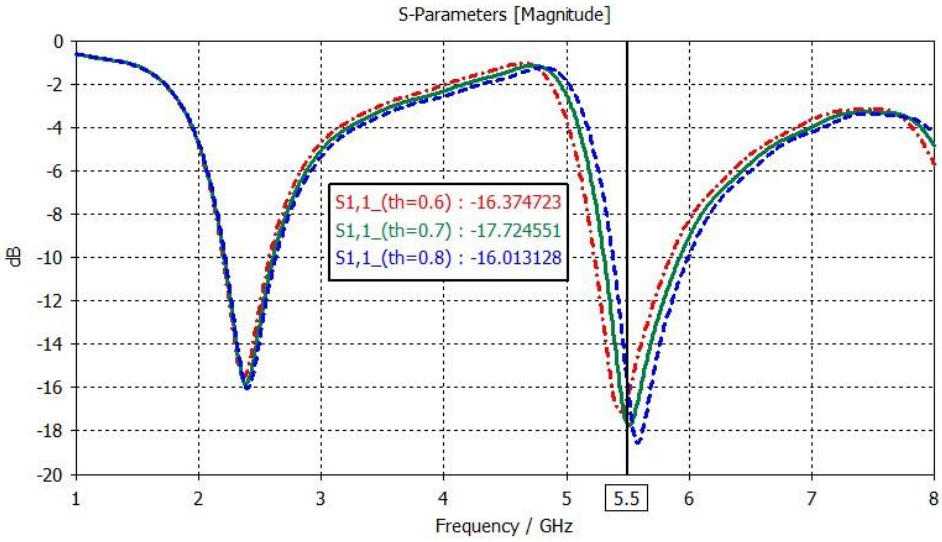

Figure 2.9 The effect of varying the thickness th on the S11

- **Effect of varying Lg1**

The simulation results of the effect of varying Lg1 on S11 are given Figure 2.10. It can be noted that changing the Lg1 value does not cause a shift for the two bands. However, increasing the value Lg1 affect negatively the matching of the two operating bands. For the considered values of Lg1, best result in terms of impedance matching for both bands, are achieved for Lg1 equals 1 mm.

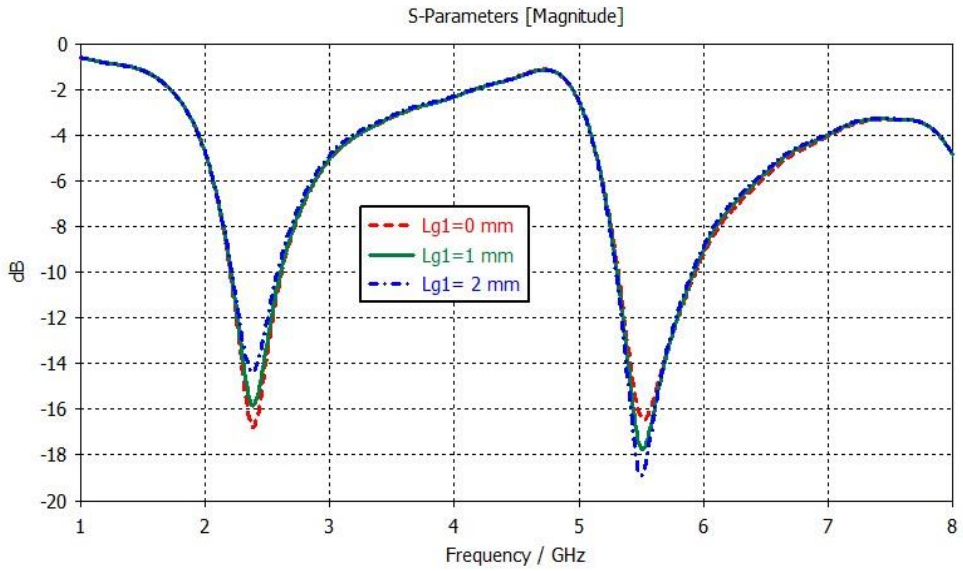

Figure 2.10 The effect of varying the length Lg1 on the S11

- **Effect of varying the wg1**

Figure 2.11 presents the simulation results for S11 for different values of Lg1. It can be noted that increasing wg1 results in good matching with slightly larger bandwidth for the second band. Therefore, wg1 controls the matching of the second band. The considered value for wg1 is 5 mm.

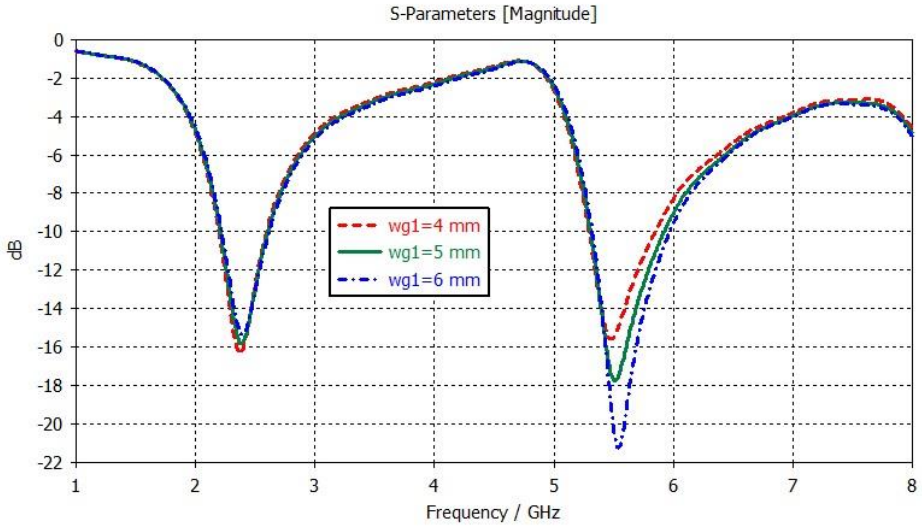

Figure 2.11 The effect of varying wg1 on the S11

2.6 Fractal Antenna Loaded with Stub

To further enhance the matching of the two operating bands and improve operating frequency bandwidths a rectangular stub is attached to the base of the radiating element of Antenna 2 and resulted structure, depicted in Figure 2.12 namely Antenna 3 .

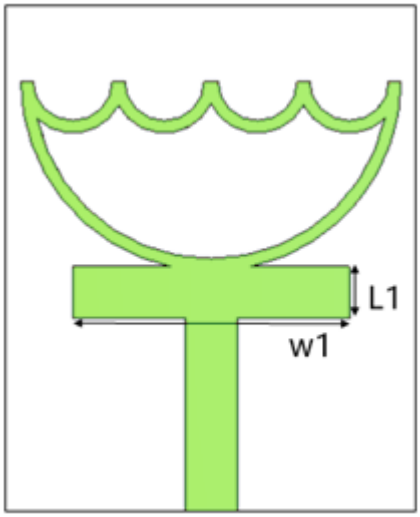

Figure 2.12 the geometry configuration of Antenna 3

2.6.1 Simulated Reflection Coefficient

Figure 2.13 shows the simulated reflection coefficient for Antenna 3. It can be observed the first operating band rages from 2.3 GHz to 2.82 GHz, with resonant frequency centered at 2.53 GHz and a reflection coefficient level of -20.23 dB. While, the second band extends from 4.94 GHz to 7.3 GHz, with a resonance frequency at 5.41 GHz and a reflection coefficient level of -37.34dB.

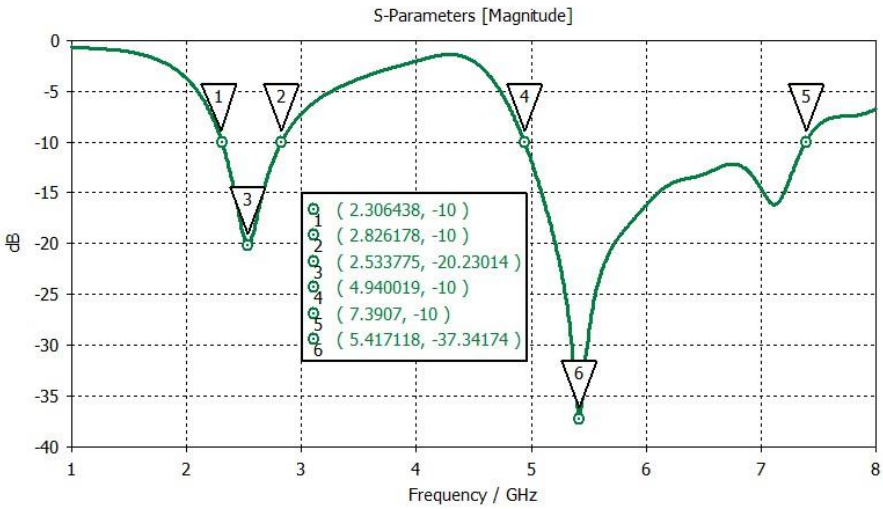

Figure 2.13 The reflection coefficient for Antenna 3 with w1 =3mm, L1=7.5mm

Since, in this part, the rectangular stub is the main change in design process, its two parameters W1 and L1 are selected to perform the sensitivity study.

- **Effect of varying the stub width w1**

Figure 2.14 presents the S11 simulated results for various stub width w1. It can be observed that changes in w1 have almost no effect on the first band. However, by increasing w1 the second bandwidth is significantly improved. Further reduction results a decreasing in bandwidth. Therefore, the considered value for w1 is 7.5 mm.

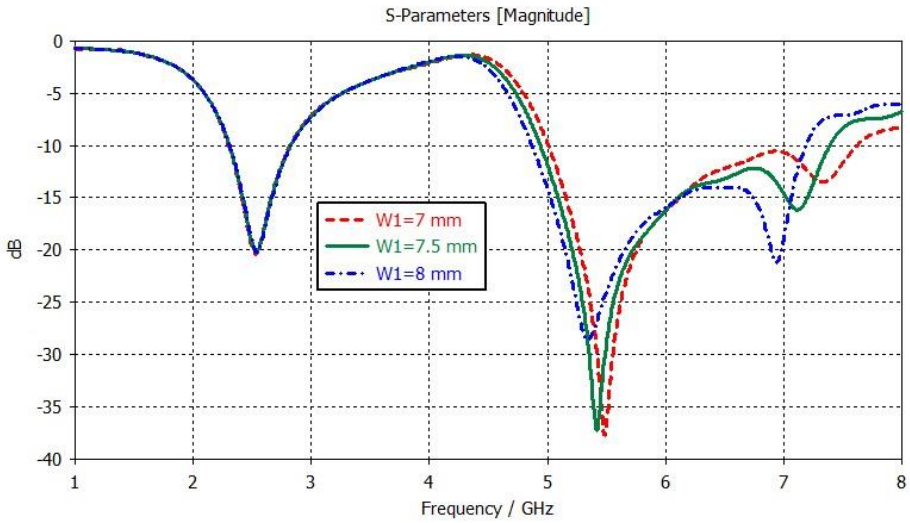

Figure 2.14 The effect of varying the width w1 on the S11

- **Effect of varying the stub length L1**

The effects of parameter L1 on the input impedance are simulated and shown in Figure 2.15. The results show that the stub length L1 mainly influences the matching of both operating bands. It is observed that a large bandwidth with good matching and resonant frequency centered at 5.5 GHz are obtained when L1=3 mm.

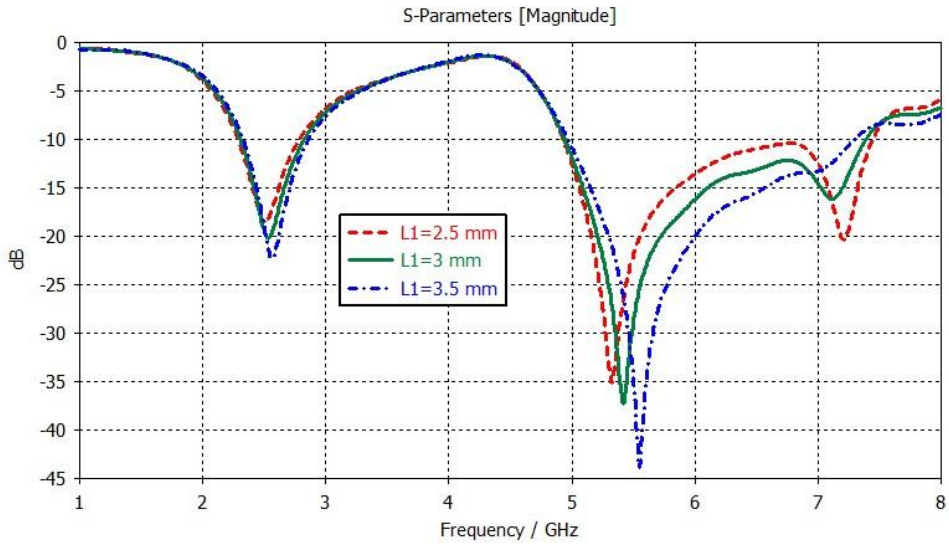

Figure 2.15 The effect of varying the length L1 on the S11

2.7 Comparison between Different Stages

The evolution stages of the proposed antenna are performed in four different steps, as illustrated in Figure 2.16. The first stage involves the use of a semicircular radiating element to create the 2.4GHz WLAN band. In the second stage, a smaller additional radiating elements need to be attached to the semicircular-shaped structure in order to cover the second band operating in the 5.5 GHz WiMAX band. However, the resulting design needs third stage of semicircular radiating element to reach the desired frequency. Moreover, the resulting design exhibits weaknesses in terms of bandwidth. To address this, the fourth stage introduces the addition of a stub to improve performance. The simulated reflection coefficient versus frequency for the proposed antenna for the four stages are shown in Figure 2.17.

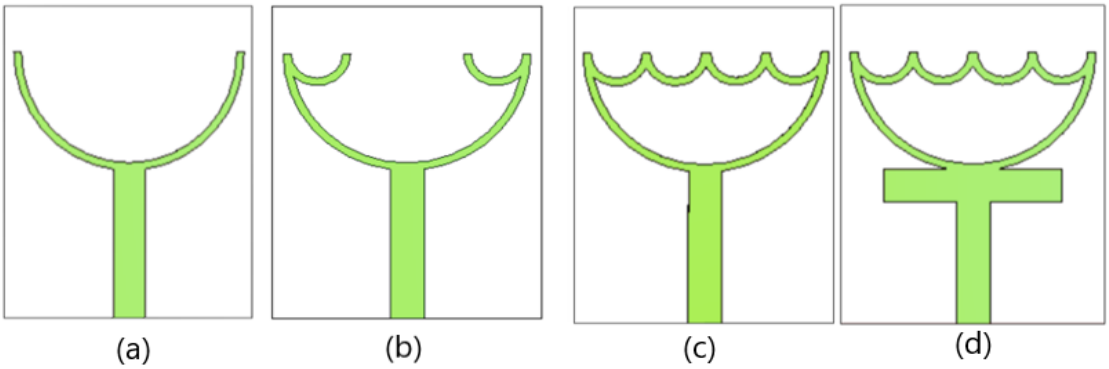

Figure 2.16 Antenna evolution (a Antenna 0 (b)Antenna 1 (c) Antenna 2 (d) Antenna 3

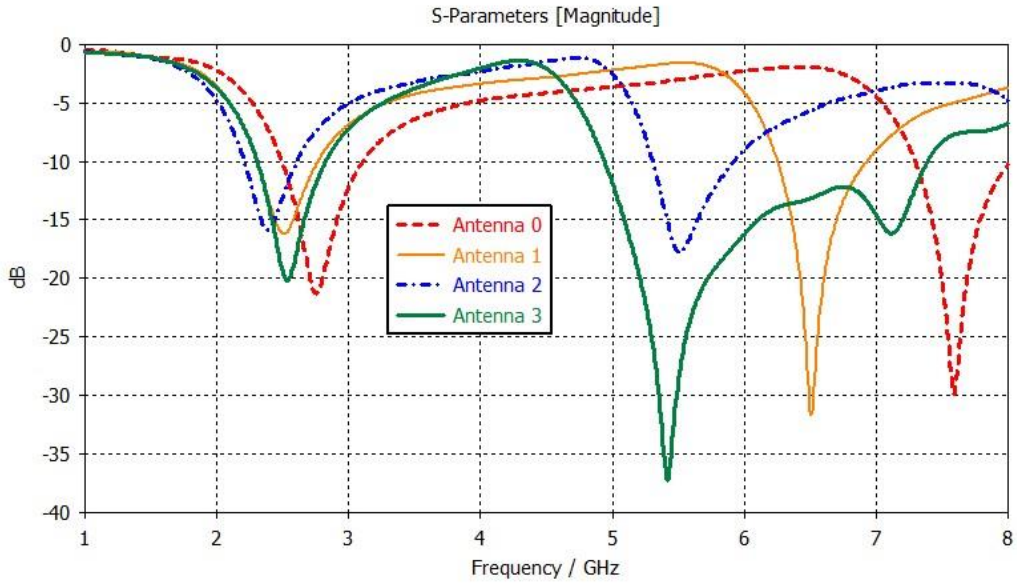

Figure 2.17 Simulated S11 for (a)Antenna 0 (b)Antenna 1 (c)Antenna 2 (d) Antenna 3

2.8 Simulation Results

2.8.1 Current Distribution

The simulated surface current distribution of the proposed fractal antenna at 2.53 and 5.41 GHz resonant frequencies are displayed in Figure 2.18 and Figure 2.19 respectively. It can be observed that, for the first resonant frequency, the current is mostly concentrated on the feedline, the outer semicircular branches and stub. Moreover, the inner semicircular arms have slight effect since the current there tends towards zero. However, for the second resonant frequency, it can be noticed that high concentration of current is recorded of the whole structure.

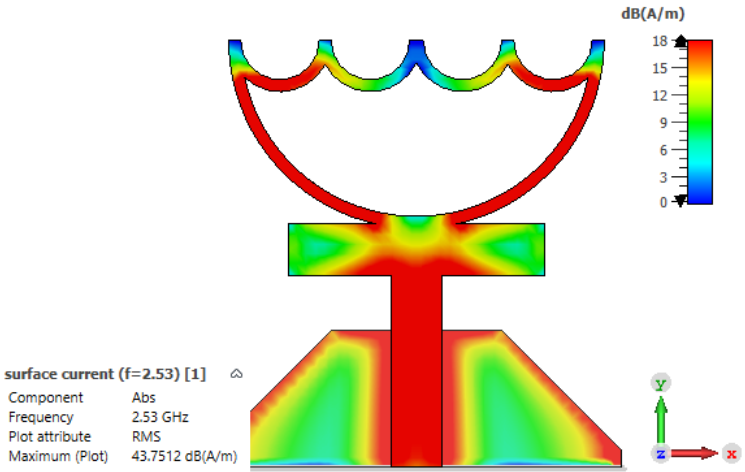

Figure 2.18 Simulated current distribution on the antenna at 2.53GHz

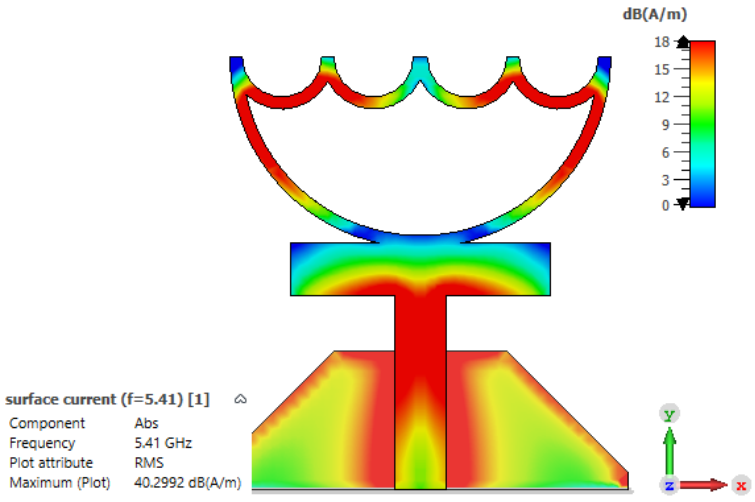

Figure 2.19 Simulated current distribution on the antenna at 5.41GHz

2.8.2 The 2D Radiation Patterns

Simulated radiation patterns in the E-and H-plane of the proposed antenna at frequencies 2.53 and 5.41 GHz are illustrated in Figure 2.20 and 2.21 respectively. At both resonant frequencies, the antenna has an omnidirectional pattern in the H-plane and a dipole-like radiation in the E-plane.

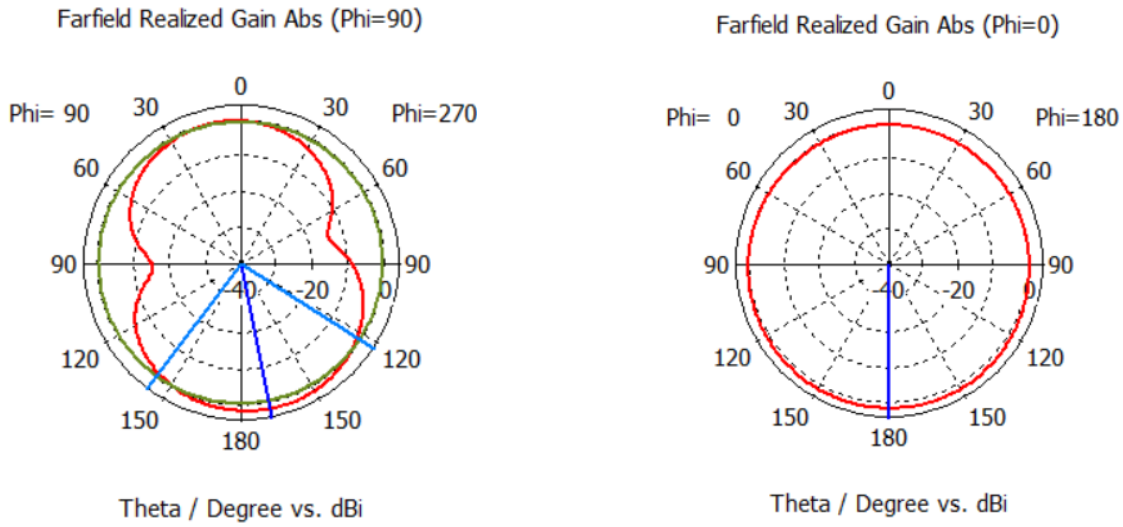

(a) (b)

Figure 2.20 2D Radiation patterns at 2.53GHz a) E-plane b) H-plane

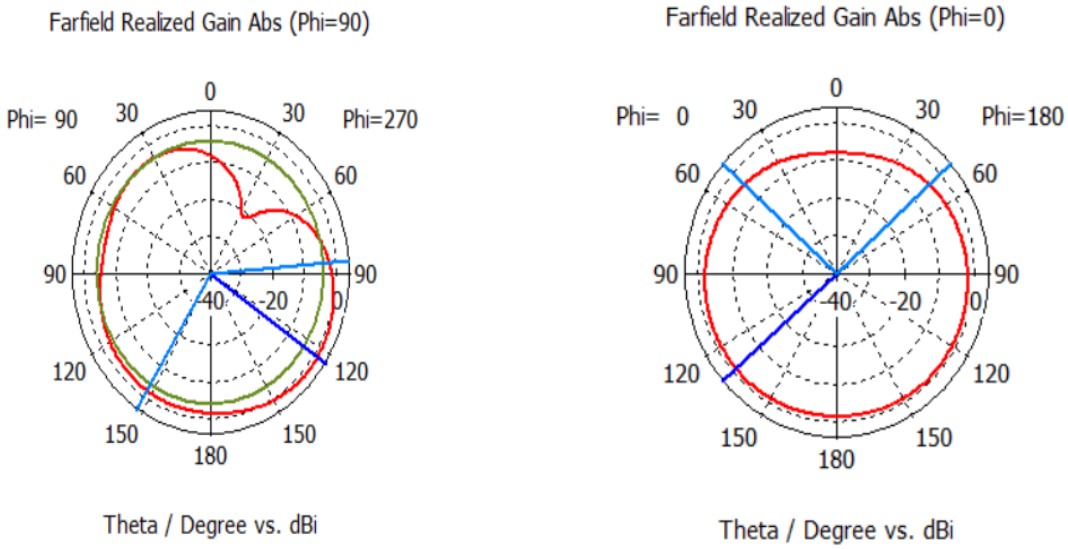

(a) (b)

Figure 2.21 2D Radiation pattern at 5.41GHz a) E-plane b) H-plane

2.8.3 The 3D Radiation Patterns

Figure 2.22 and Figure 2.23 shows the simulated 3D radiation patterns of Antenna 3 at 2.53 GHz and 5.41 GHz respectively. At the low resonant frequency, the antenna exhibits with a peak gain of 1.37 dBi. While at high resonant frequency the antenna exhibit with maximum gain of 0.75 dBi.

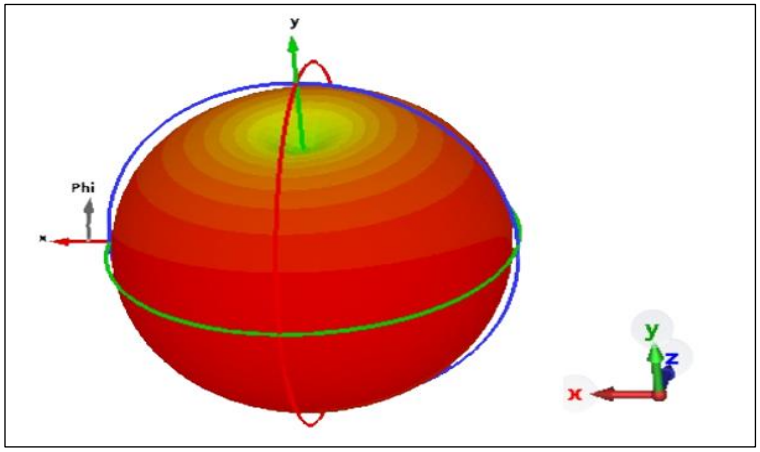

Figure 2.22 3D Radiation pattern at 2.53GHz

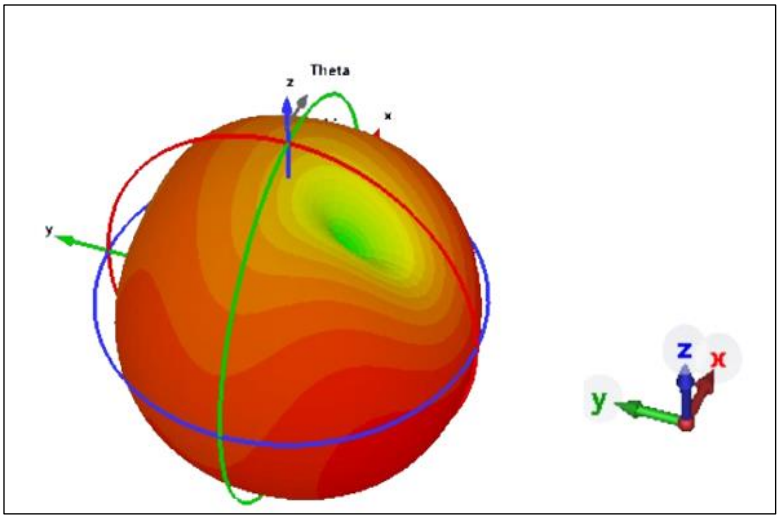

Figure 2.23 3D Radiation pattern at 5.41GHz

2.9 Experimental Results

2.9.1 Realization of the Second Proposed Dual-Band Fractal Antenna

The proposed antenna is fabricated and tested. The reflection coefficient is measured using the Vector Network Analyzer (VNA) scanning the range of frequencies from 100 MHz to 20 GHz available at the Institute IGEE. The photograph of the top and bottom views of the realized antenna is shown in Figure 2.24.

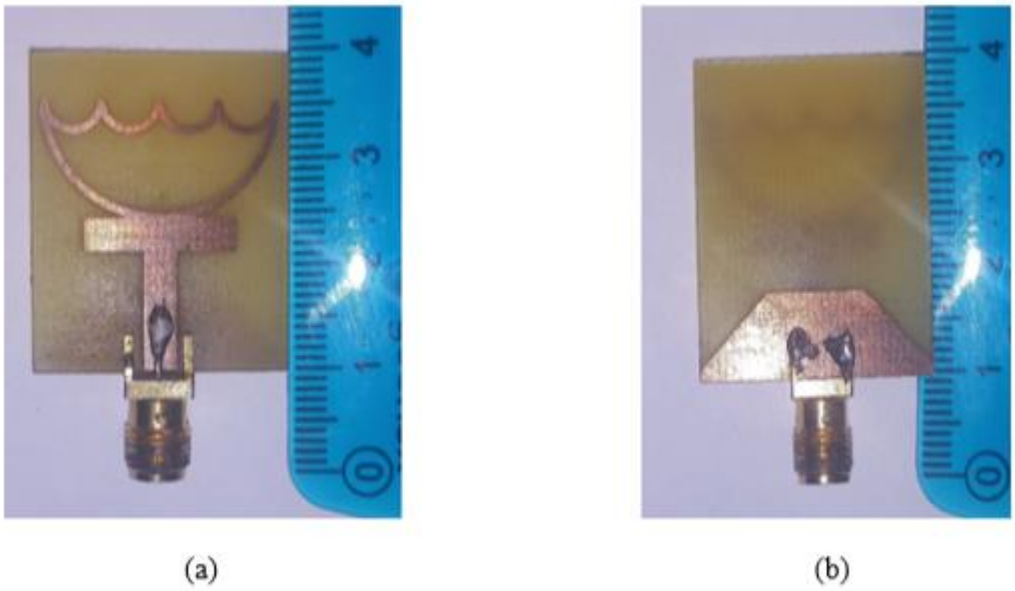

Figure 2.24 Fabricated proposed antenna (a) top view and (b) bottom view.

2.9.2 Comparison between the Simulated and Measured S11

Comparing the graphs of the measured and simulated reflection coefficients in dB appearing in Figure 2.25. It is deduced that the results indicate an overall agreement. It can be seen that, the measured lower frequency band extends from 2 GHz to 2.6 GHz with resonant frequency centered at 2.4 GHz, which cover widely the 2.4 WLAN application. Moreover, the measured impedance bandwidth of the second band extends from 5.4 GHz to the band 8 GHz with a resonant frequency centered at 6 GHz which also covers the 5.5GHz WiMAX and 5.6/5.8GHz WLAN applications

The difference between the measured and simulated results mainly due to the manufacturing tolerances and precision, the non-exact value of the thickness and the dielectric substrate relative permittivity and the SMA connector quality.

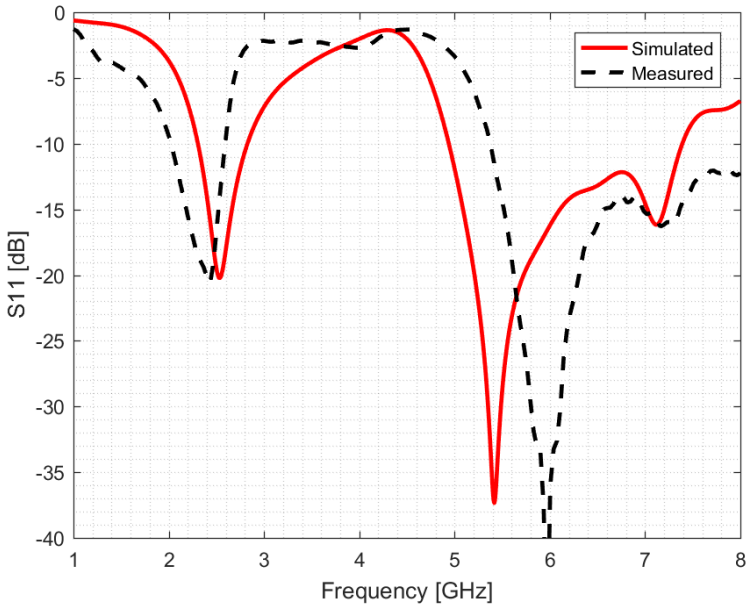

Figure 2.25 Simulated and measured reflection coefficient in dB versus frequency.

2.10 Conclusion

In this chapter, a fractal dual-band antenna has been designed to cover the 2.4 GHz WLAN and 5.5 GHz WiMAX operating bands. A stepwise procedure and parametric studies of the most important parameters have been conducted to achieve the optimal design. The resulting design covers a wide range of frequencies, including the 2.4/5.6/5.8 GHz WLAN bands and 5.5GHz WiMAX band, as well as the 5.9 GHz to 7.1 GHz range used for 5G applications in USA [14]. The proposed antenna is simulated, fabricated and measured. In the next chapter, another approach to design dual-band fractal antenna will be presented.

Chapter three: Design of a Fractal Antenna Based on ω-Shaped Strip Line

Design of a Fractal Antenna Based on ω-Shaped Strip Line

3.1 Introduction

In the previous chapter, we presented a fractal dual-band antenna that is intended to operate in two bands, covering the 2.4 GHz WLAN and 5.5 GHz WiMAX operating bands. In this chapter, another approach is used to design a dual-band antenna based on ω-shaped radiating arms.

The following sections provide a step-by-step procedure, beginning with a ω-shaped antenna with specific dimensions, leading to a second stage fractal antenna based on ω-shaped branches.

3.2 ω-shaped Microstrip Antenna

The proposed structure named 'Ant 0' comprises of a ω-shaped radiating element with radius S1 of each semicircular arm attached to a 50Ω transmission line with width wf and length Lf printed in the front side of the FR-4 substrate. In the back side of the substrate there is a tapered ground plane with larger width of w, smaller width of wg and length Lg as can be seen in Figure 3.1. The dimensions of the proposed design are summarized in Table 3.1.

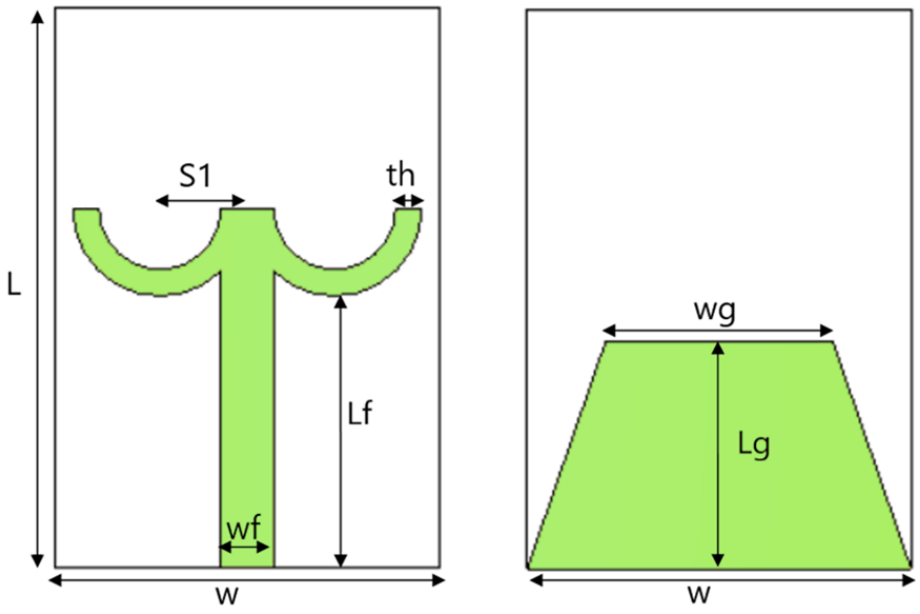

Figure 3.1 Geometrical configuration of Ant 0 (a) Front view (b)bottom view

Table 3.1 The Dimensions of the Proposed ω-shaped Antenna.

Parameter	S1	th	wf	wg	Lg	Lf	L	W
Value (mm)	5	1.5	3	13	13	15.5	32	22

3.2.1 Simulated Reflection Coefficient

The simulated reflection coefficient is presented in Figure 3.2. It can be noticed that the antenna operates in a wide frequency band ranging from 3.15 GHz to 6.21 GHz. Notably, the antenna demonstrates two resonant frequencies at 3.66 GHz and 5.3 GHz with a reflection coefficient level of -14.18dB and -23.037dB, respectively.

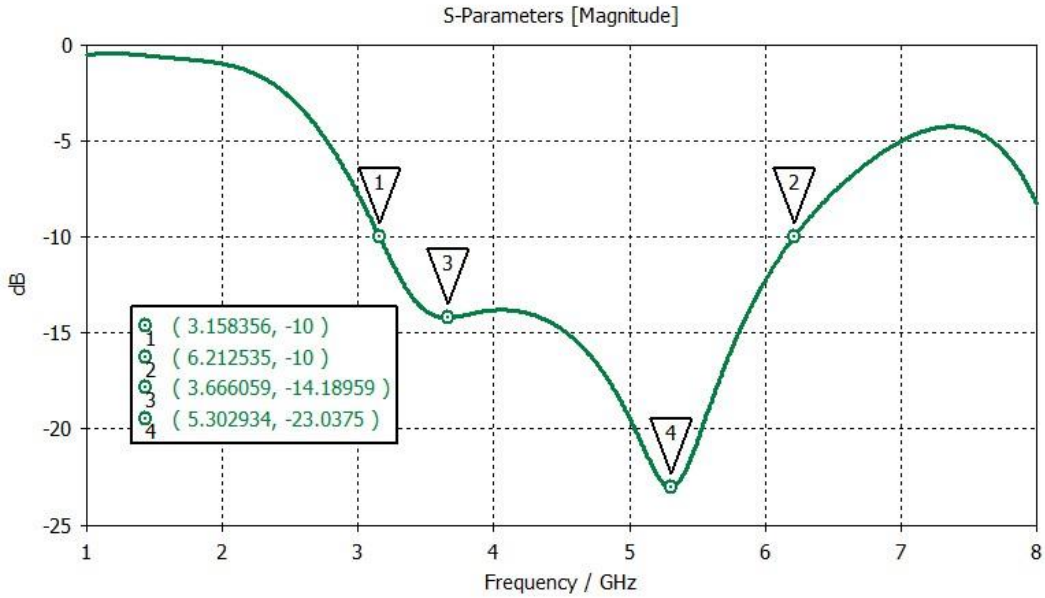

Figure 3.2 The reflection coefficient for Ant 0

3.3 *Fractal Antenna Based on Dual ω*-shaped Radiating Element

In the aim of covering the 2.4 GHz WLAN, another ω-shaped arm is attached to Ant 0 to design Ant 1, as depicted in Figure 3.3. It is worth to mention that all the antenna dimensions are kept constant as in Ant 0.

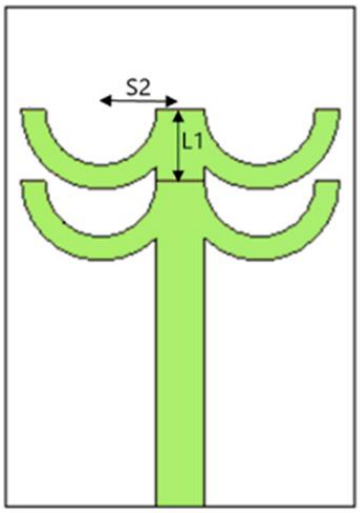

Figure 3.3 Gemetry configuration of Ant 1

3.3.1 Simulated Reflection Coefficient

The simulated reflection coefficient for Ant 1 is presented in Figure 3.4. It can be clearly seen that the structure operate in two large bands. The first operating band ranges from 2.54 GHz to 3.25 GHz with resonance frequency centered at 2.83 GHz and a S11 level of -22.07 dB. However, the second band extends from 4.08 GHz to 6.7 GHz with a resonance frequency of 5.54 GHz and a S11 level of -51.21 dB. In can be concluded that Ant 1 do not cover the requested band.

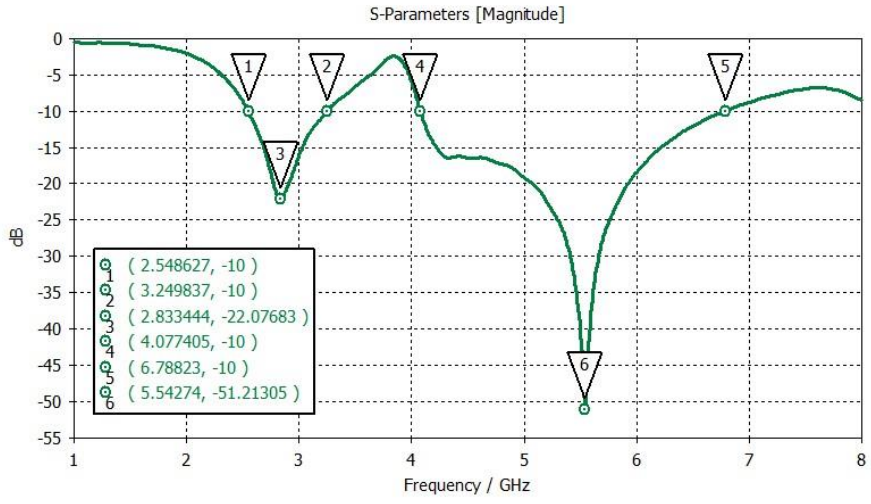

Figure 3.4 The reflection coefficient for Ant 1 for S2= 5 mm and L1= 4.5 mm

- **Effect of varying raduis S2**

In the aim of covering the 2.4 GHz WLAN band, the radius of the semicircular arms are varied. Figure 3.5 shows the simulation results with different values of S2. It can be concluded

that by increasing S2, the first frequency band moves toward lower frequencies. As for the second band, the lower cut off frequency decreases leading to wider operating frequency band. The value S2=5 mm is chosen since it is the largest value before the overlapping of the structure branches.

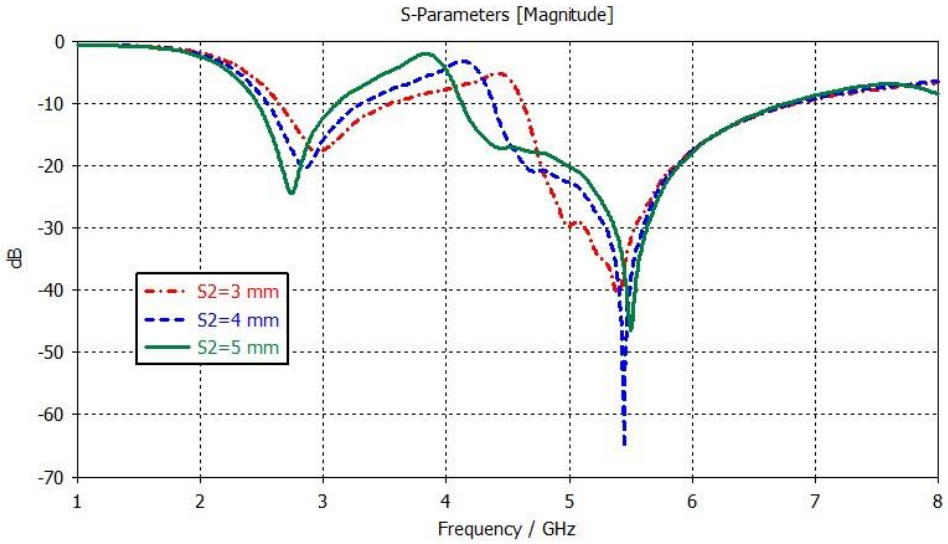

Figure 3.5 The effect of varying the radius S2 on the S11

3.4 Fractal Antenna Based on Triple ω-Shaped Radiating Element

Since the previous modifications on the antenna structure are not able to bring down the first operating band so that its covers the 2.4 GHz WLAN, a third ω-shaped branch is attached to Ant 1 to design Ant 2, as shown in Figure 3.6.

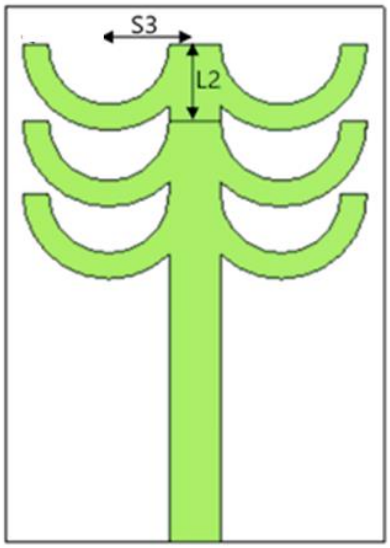

Figure 3.6 Gemetry configuration of the Ant 2

3.4.1 Simulated Reflection Coefficient

The simulated reflection coefficient for Ant 2 is shown in Figure 3.7. It is clearly seen that 2.4 GHz WLAN band is largely covered. Furthmore, the second band operating band extends from 4.05 GHz to 6.89 GHz and hence covering the 5.5 WiMAX and 5.2 /5.6/5.8 GHz WLAN applications and the 5.9 GHz to 6.4 GHz range used for 5G applications [14].

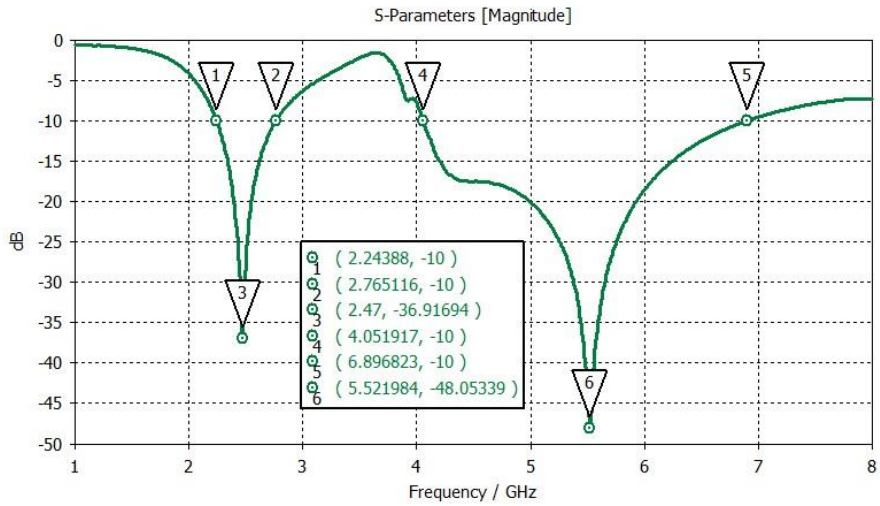

Figure 3.7 The reflection coefficient for Ant 2 for S3= 5 mm and L2= 4.5 mm

- **Effect of varying S3**

The effects of parameter S3 on the input impedance are simulated and shown in Figure 3.8. The results shows that the increasing of S3 shifts the first frequency band toward lower frequencies with an increase in the bandwidth of the second frequency band. The value S3=5 mm is chosen since it is achieving the 2.45 GHz frequency.

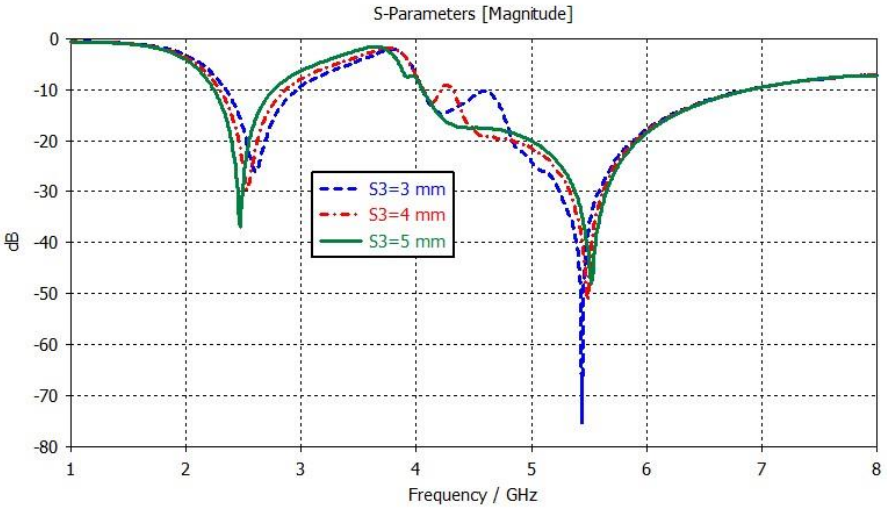

Figure 3.8 The effect of varying the radius S3 on the S11

- **Effect of varying the L2**

By increasing L2 there will be a small shift in the first frequency band toward lower frequencies without affecting the second band as shown in Figure 3.9. However, the smallest value, L2=4.5 mm, is chosen since it reaches the 2.45GHz.

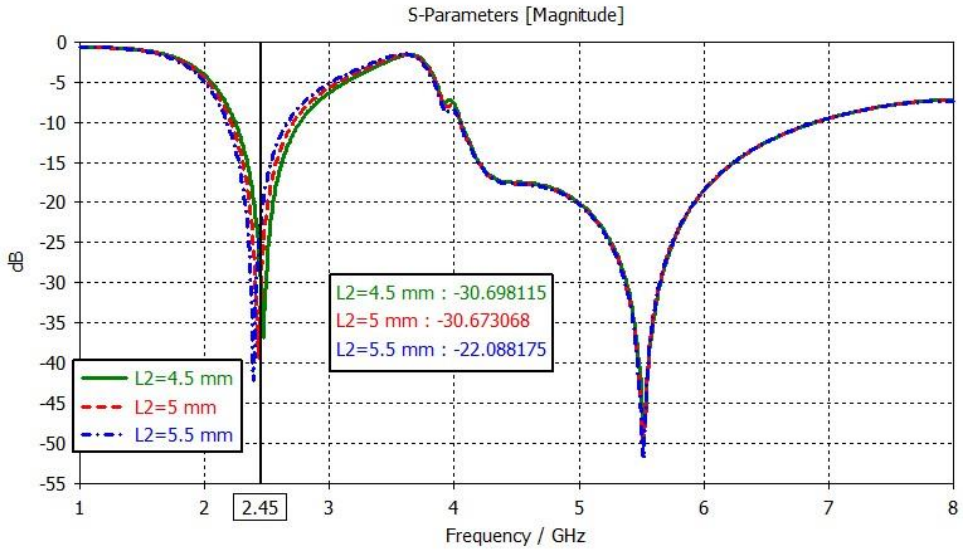

Figure 3.9 The effect of varying the L2 on the S11

- **Effect of varying Lf**

Figure 3.10 displays the effect of varying the feedline length Lf on the S11response. As Lf increases from 13mm to 15 mm with step of 1 mm, the matching of the both bands is affected

and lead to reducing operating frequency bands. Therefore, Lf=14 mm provides optimum results which meet the applications requirements.

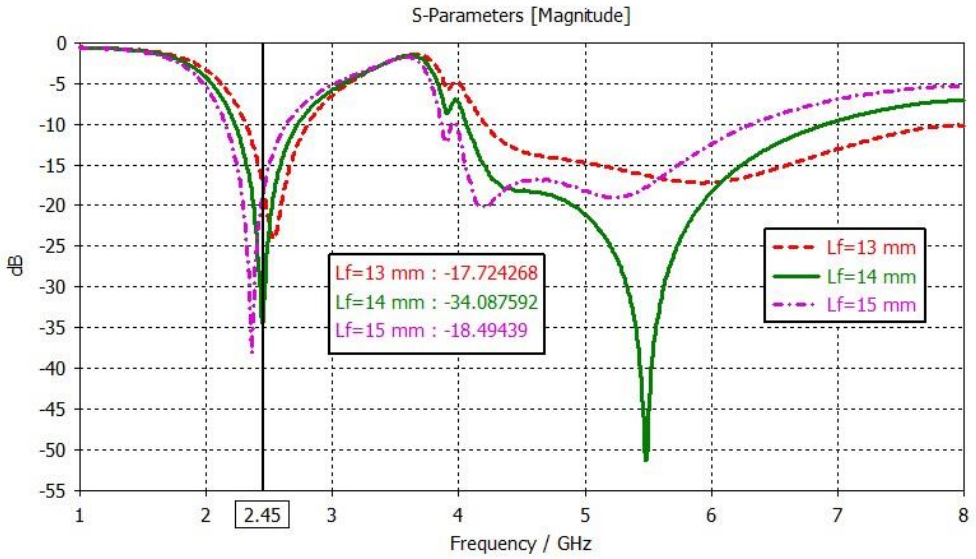

Figure 3.10 The effect of varying Lf on the S11

- **Effect of varying the arms thickness th**

The simulated reflection coefficient for different values of th are depicted in Figure 3.11. It is clear from the simulation results that a significant effect on the second band and slight changes in the first band. Good impedance matching with closest resonant frequencies to the required resonant frequencies (2.45 GHz and 5.5 GHz) is achieved when th = 1.5 mm.

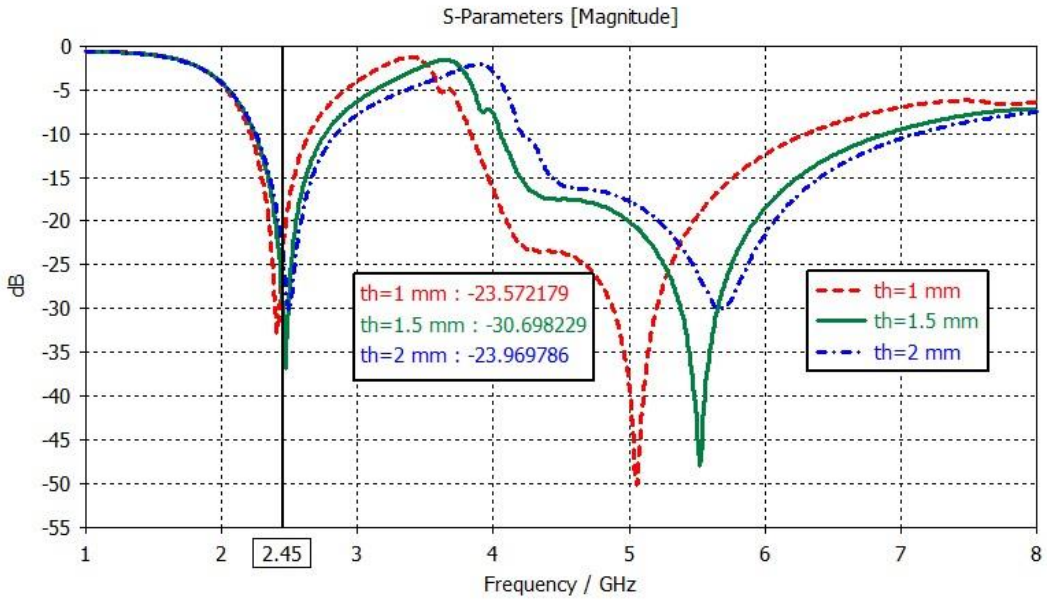

Figure 3.11 The effect of varying th on the S11

3.5 Comparison between Different Stages

The evolution stages of the proposed antenna are performed in three different steps, as illustrated in Figure 3.12. The first stage involves the use of a *ω*-shaped that has a wide band including the 5.5GHz WiMAX band. In the second stage, fractal antenna based on dual **ω**-shaped radiating element is added to cover the 2.4 GHz WLAN band. However, the resulting design is not reaching the desired band. To address this, the third stage introduces fractal antenna based on triple **ω**-shaped radiating element. The simulated reflection coefficient versus frequency for the proposed antenna for the three stages are shown in Figure 3.13.

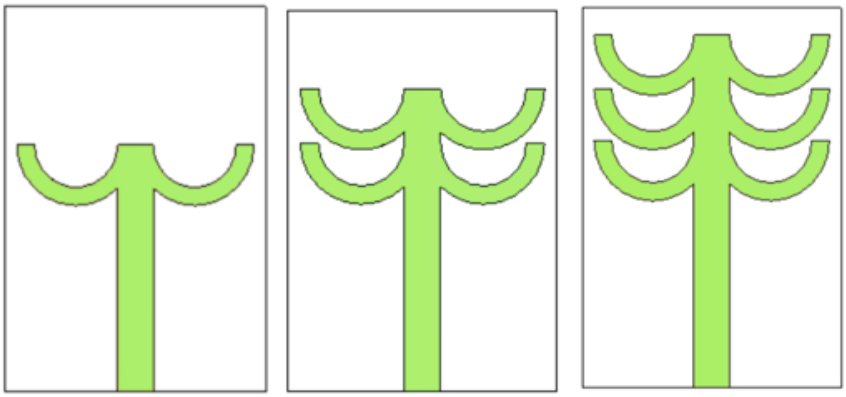

(a) *(b)* *(c)*

Figure 3.12 the design evolution (a) Ant 0 (b) Ant 1 (c) Ant 2

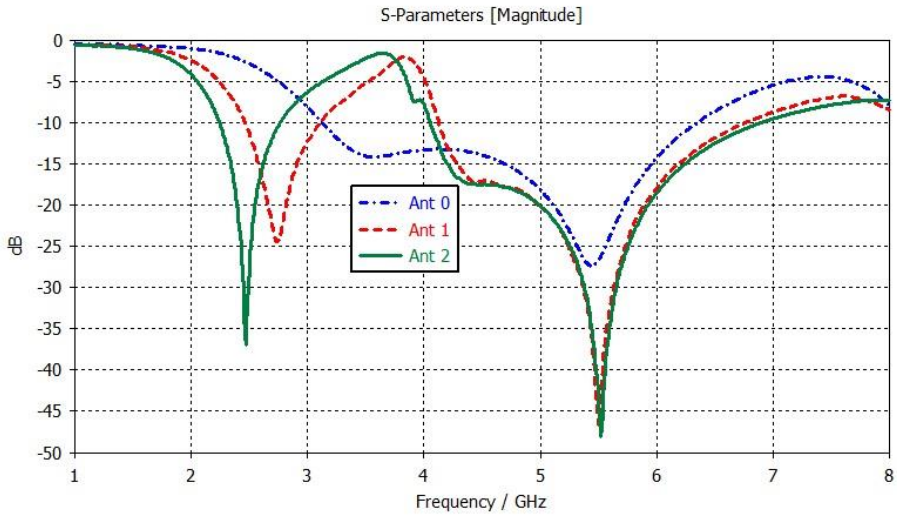

Figure 3.13 The reflection coefficient for Ant 0, Ant 1 and Ant 2

3.6 Simulation Results

3.6.1 The Current Distribution

The simulated surface current distribution of the proposed fractal antenna at 2.47 and 5.52 GHz resonant frequencies are displayed in Figure 3.14 and Figure 3.15 respectively. It can be observed that, at the first resonant frequency, the current is mostly concentrated on the feedline and on the third ω-Shaped arm. Moreover, it is almost zero at the end of the first and the second arms. However, at the second resonant frequency, it can be noticed that high concentration of current is recorded on the feedline and on the bottom arms of the antenna radiating patch.

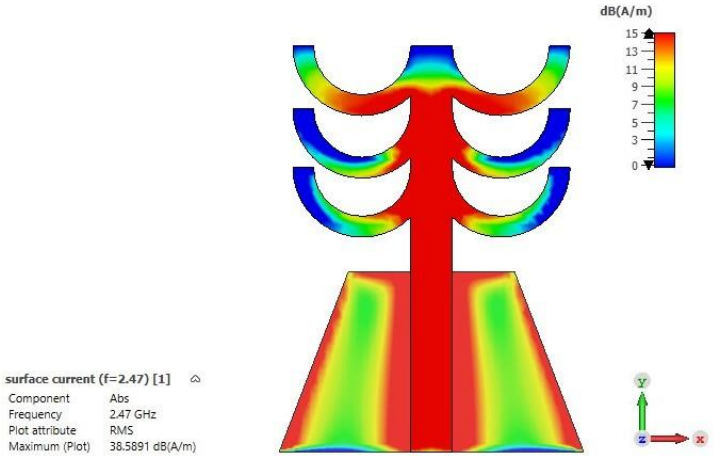

Figure 3.14 Simulated surface current on Ant2 at 2.47 GHz

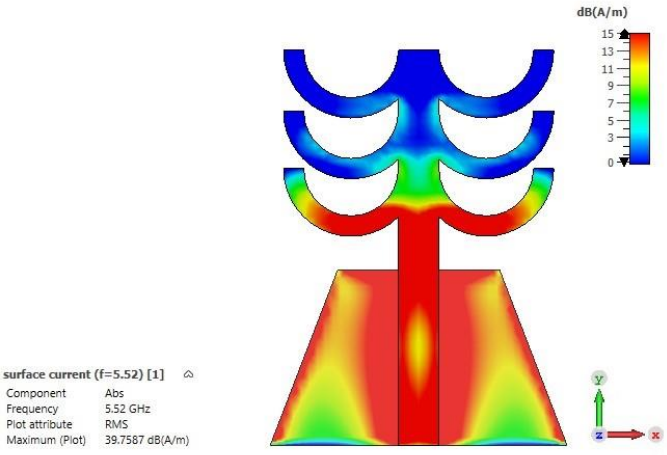

Figure 3.15 Simulated surface current on Ant 2 at 5.52 GHz

3.6.2 The 2D Radiation Patterns

The simulated E-and H-plane of the proposed antenna at frequencies 2.47 and 5.52 GHz are illustrated in Figure 3.16 and 3.17 respectively. At both resonant frequencies, the antenna shows an omnidirectional pattern in the H-plane and a dipole-like radiation in the E-plane.

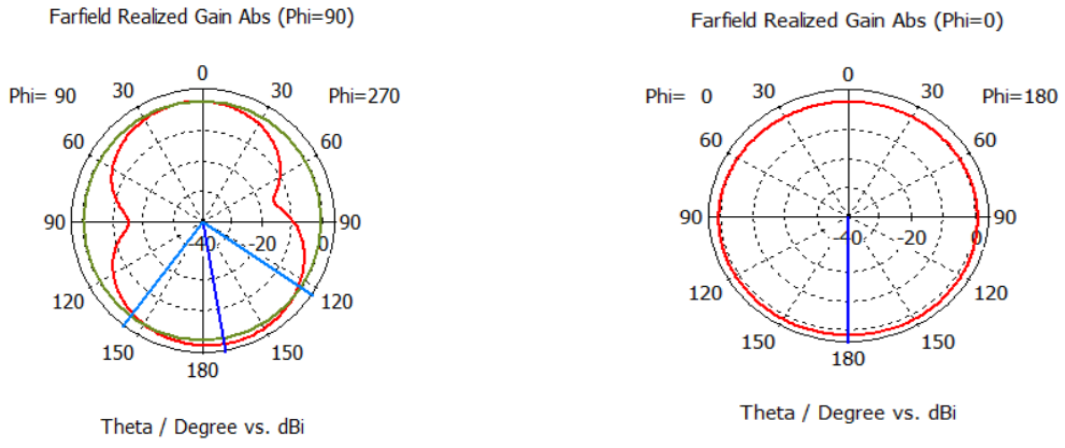

(a) (b)

Figure 3.16 The 2D radiation patterns at 2.47 GHz a) E-plane b) H-plane

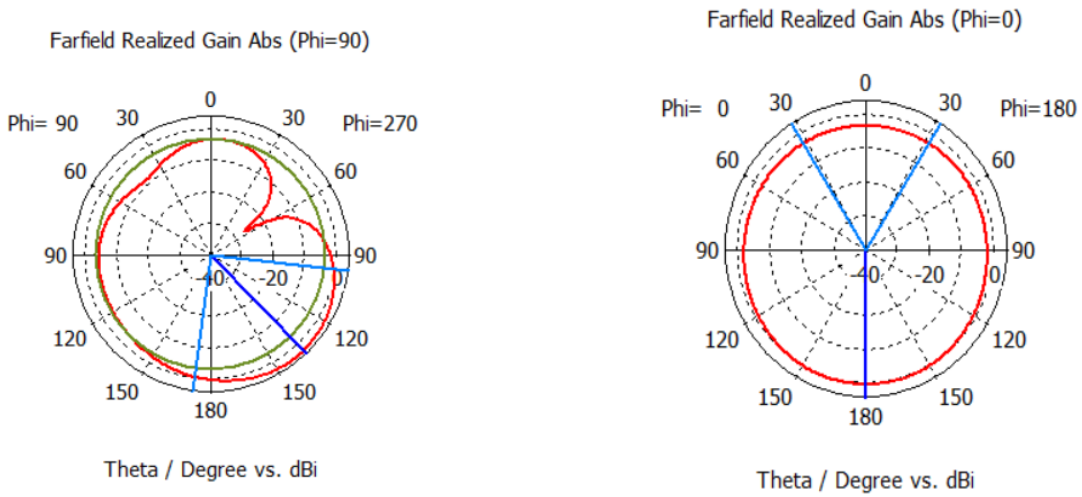

(a) (b)

Figure 3.17 The 2D radiation patterns at 5.52 GHz a) E-plane b) H-plane

3.6.3 The 3D Radiation Patterns

Figure 3.18 and Figure 3.19 shows the simulated 3D radiation patterns of Ant 2 at 2.47 GHz and 5.52 GHz respectively. At the low resonant frequency, the antenna exhibits a peak gain of 1.484dBi. While at high resonant frequency, the antenna exhibits a maximum gain of 2.3dBi

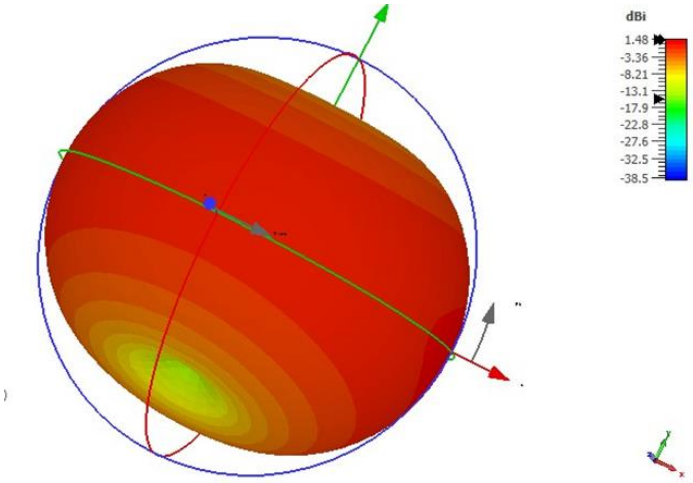

Figure 3.18 The 3D radiation patterns at 2.47GHz

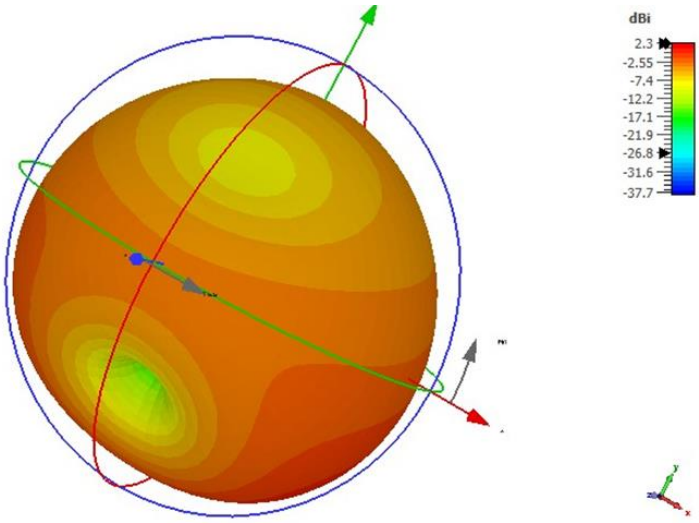

Figure 3.19 The 3D radiation patterns at 5.52GHz

3.7 Experimental Results

3.7.1 Realization of The Second Proposed Antenna

Using the optimized parameters given in the previous section, the propped antenna is fabricated and tested. The photograph of the prototyped structure is shown in Figure 3.20.

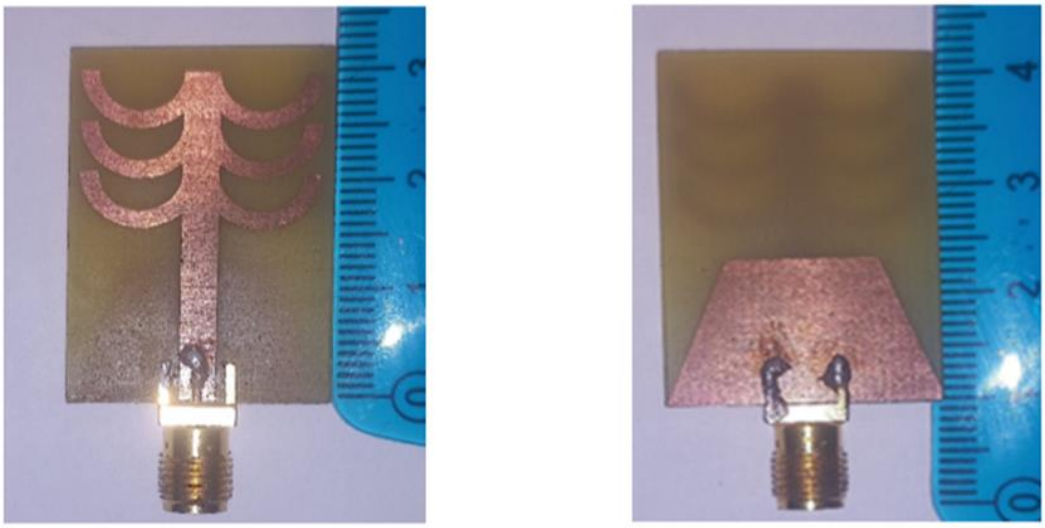

Figure 3.20 Fabricated proposed antenna (a) top view and (b) bottom view.

3.7.2 Comparison between The Simulated and Measured S11

The simulated and measured S11 are depicted in Figure 3.21. It can be seen that both results agree closely with each other. The measured results show that the proposed antenna has 10-dB impedance bandwidth of 800 MHz (2–2.8 GHz) and 2.4 GHz (4–6.4 GHz). The slight difference seen between the simulated and the measured results is basically due to the manufacturing tolerances, the uncertainty of the thickness and dielectric relative constant of the substrate, the quality of the SMA connector, and to the imperfect experimental environment.

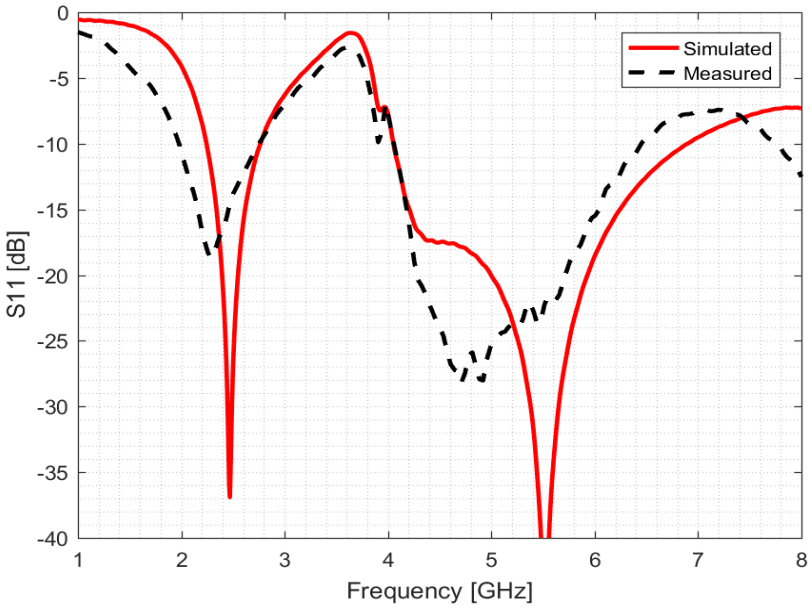

Figure 3.21 Simulated and measured reflection coefficient versus frequency

3.8 Comparison between the Two Proposed Antennas and Related Works

To see how well the proposed fractal dual band antennas are, a comparison is established between them with other works.

Table 3.2 Comparison between the proposed antennas and related works

	Size (mm^3)	***Operating bands (GHz)***	***S11 level (dB)***	***Bandwidth percentage (%)***	***Maximum Gain (dBi)***
[15]	75× 75× 1.6	[2.4 - 2.53] 2.45 [5.05 -5.81] 5.3	-18.3 -23.2	9.38 23.7	7.65 7.24
[16]	20 × 40 × 1.6	[2.37 - 2.41] 2.4 [5.72 - 5.88] 5.8	-16.1 -12.1	1.66 2.2	*0.4* *-1.6*
The first antenna	24×29.5×1.6	[2.3 - 2.82] 2.53 [4.94 -7.3] 5.41	-20.23 -37.34	20.31 38.56	1.37 0.75
The second antenna	22×32×1.6	[2.24- 2.76] 2.47 [4.05 -6.89] 5.52	-36.91 -48.05	20.8 51.92	1.484 2.302

As can be concluded from the table, the two antennas has small difference in their sizes. However, the second proposed antenna gives much better results comparing to the first one in term of bandwidth and gains. Moreover, the proposed antenna gives much better results comparing to other antennas.

Final Conclusion

In this project, compact dual-band fractal antennas for WLAN/WIMAX applications have been presented. The proposed geometries are based on semicircular radiating arms. The combination of the branches in two deferent fractal approaches has led to two different structures.

The first proposed antenna design process begins with semicircular-shaped patch leading a comb-shaped fractal antenna with a stub operating in two different bands covering the 2.4/5.2 /5.8 GHz WLAN bands and 5.5 GHz WiMAX band, as well as the 5.9 GHz to 7.1 GHz 5G applications. The simulated radiation pattern is omnidirectional in both operating bands. Furthermore, the antenna has very compact with an overall dimension of only 24 × 29.5 mm^2. The design has been simulated and tested and it has shown satisfactory results.

A second design of a dual-band fractal antenna has been also proposed. This design consisted of three interconnected identical ω-shaped arms to create two resonance frequencies. The structure has also a compact size with overall dimension of 22 × 32 mm^2. Moreover, the proposed design operates in two bands [2.24-2.72 GHz] and [4.05.-6.89 GHz] and covers the 2.4/5.2/5.8 GHz WLAN bands and 5.5 GHz WiMAX, as well as the 5.9 GHz to 6.4 GHz 5G applications. The design has been also simulated and tested and it has shown satisfactory results.

Finally, a comparison it terms of radiation characteristic between the proposed antennas has showcased several favorable attributes, including wide operating bands, broad bandwidth, good impedance matching, overall size and the maximum gain.

References

[1] D. H. P. a. G. D. Makwana, "A Comprehensive Review on Multi-band Microstrip Patch," *International Journal of Computing and Digital Systems,* 2022.

[2] X. Yang, J. Chiochetti, D. Papadopoulos, and L. Susman;, "Fractal Antenna Elements and Arrays," International Journal of technical feature 1999.

[3] Indrasen Singh, Dr. V.S. Tripathi, "Micro strip Patch Antenna and its Applications: a Survey," Communications and Space Sciences Laboratory 2011.

[4] S. Narinder, "A Study Of Different Feeding Mechanisms In Microstrip Patch Antenna," International Journal of Microwaves Applications, February 2017.

[5] M.R.Hire C.S.Ahire, "A Review on Microstrip Patch Antenna Design and its," International Conference on Contents, Computing & Communication, 2022.

[6] N. B. Bisht, "Study The Various Feeding Techniques of Microstrip Antenna," International Journal of Emerging Technology and Advanced Engineering, 2015.

[7] N. O. Parchin, H. J. Basherlou, R. A. A.-A. Noras and J. M., "Dual-Band Monopole Antenna for RFID Applications," Future Internet, vol. 11(2), no. 31, pp. 1-10, January 2019

[8] Anuj Mehta, "Microstrip Antenna," *International Journal of Scientific & Technology Research* , 2015.

[9] C. Balanis, Antenna theory: Analysis and design, fourth edition, New York, 2016.

[10] S. Narinder, " "A Study Of Different Feeding Mechanisms In Microstrip Patch Antenna," International Journal of Microwaves Applications," 2017.

[11] N. Abdullah, "Design of Minskowsi Fractal Antenna for Dual Band Application," dings of the International Conference on Communication Engineering 2008.

[12] Γ. Benyetho, "Design of a Novel Fractal Multiband Planar Antenna," International of Electronics and Communication Engineering Vol:9, No:1, 2015.

[13] Aya N. Alkhafaji, "Design of Flexible Dual-Band Tree Fractal Antenna for Wearable," Progress In Electromagnetics Research C, Vol. 125, 51–66, 2022.

[14] S. W. Minehane, "Spectrum Requirements for digital transformation,"The study commissioned by the federation of German Induststries (BDI) 2020.

[15] M. K. C. I. MATTSSON, "Dual-band dual-polarized full-wave rectenna based on differential field sampling," in *IEEE Antennas and Wireless Propagation Letters*, 2018.

[16] Ali MSM, Rahim SKA, Sabran MI, Abedian M, Eteng A and Islam MT "Dual band miniaturized microstrip slot antenna for WLAN applications". Microwave and Optical Technology Letters, 2018.